J Comput Neurosci
DOI 10.1007/s10827-013-0472-6

Distribution of correlated spiking events in a population-based approach for Integrate-and-Fire networks

Jiwei Zhang · Katherine Newhall · Douglas Zhou · Aaditya Rangan

Received: 22 March 2013 / Revised: 12 June 2013 / Accepted: 16 June 2013

Abstract Randomly connected populations of spiking neurons display a rich variety of dynamics. However, much of the current modeling and theoretical work has focused on two dynamical extremes: on one hand homogeneous dynamics characterized by weak correlations between neurons, and on the other hand total synchrony characterized by large populations firing in unison. In this paper we address the conceptual issue of how to mathematically characterize the partially synchronous "multiple firing events" (MFEs) which manifest in between these two dynamical extremes. We further develop a geometric method for obtaining the distribution of magnitudes of these MFEs by recasting the cascading firing event process as a first-passage time problem, and deriving an analytical approximation of the first passage time density valid for large neuron populations. Thus, we establish a direct link between the voltage distributions of excitatory and inhibitory neurons and the number of neurons firing in an MFE that can be easily integrated into population–based computational methods, thereby bridging the gap between homogeneous firing regimes and total synchrony.

Action Editor: Gaute T. Einevoll

J. Zhang · K. Newhall (✉) · A. Rangan
Courant Institute of Mathematical Sciences,
New York University, New York, USA
e-mail: newhall@cims.nyu.edu

D. Zhou
Department of Mathematics,
MOE-LSC and Institute of Natural Sciences,
Shanghai Jiao Tong University,
Shanghai 200240, China

Keywords Spiking neurons · Synchrony · Homogeneity · Multiple firing events · First passage time · Integrate and fire neuronal networks

1 Introduction

The homogeneous and synchronous dynamics of biological and model neuronal networks have received much attention over the years (Amari 1974; Amit and Brunel 1997; Bruzsaki and Draguhn 2004; Cai et al. 2006; Cai et al. 2004; DeVille and Peskin 2008; Eggert and Hemmen 2001; Fusi and Mattia 1999; Gerstner 1995; 2000; Knight 1972; Newhall et al. 2010; Nykamp and Tranchina 2000; Omurtage et al. 2000; Singer 1999; Treves 1993; Wilson and Cowan 1972; 1973), but it is perhaps what lies in between that gives rise to their rich dynamics. In this paper, we consider a regime of apparent and sudden barrages of firing that are temporally localized and are separated by time spans of homogeneous firing (c.f. Fig. 1). These spurts of firing activity involving different groups of neurons (ranging from a few neurons to a substantial fraction of the population) are called multiple firing events (MFEs) (Rangan and Young 2013a), and can not be described as either synchronous or homogenous firing events. These events are generally initiated by one excitatory spiking neuron that in turn causes some subset of other neurons to fire, reflecting the strong correlation between firing activity. The complicated structures of MFE dynamics have not only been observed in experimental studies of a variety of animals, including the leech ganglia, rat hippocampus, as well as the olfactory system of moths, the auditory cortex of rats and the visual cortex of the monkey and the cat (Churchland and et al. 2010; DeWeese and Zador 2006;

Published online: 13 July 2013

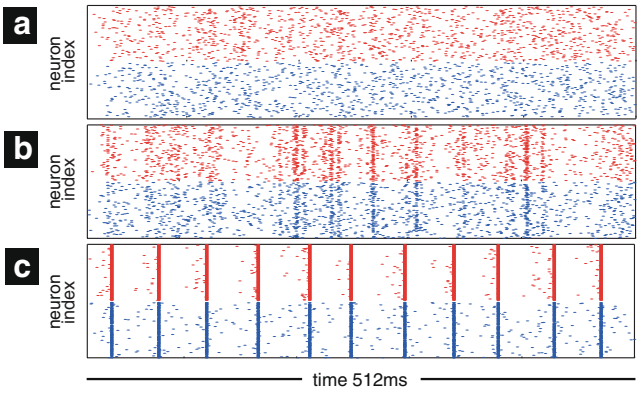

Fig. 1 (Color online) Raster plots for excitatory (*red - top half*) and inhibitory (*blue - bottom half*) neuron populations demonstrating three regimes that the I&F model can operate in: **a** a homogeneous regime with little to no correlations between spike times, $S^{EE} = S^{EI} = S^{IE} = S^{II} = 0.003$, **b** an MFE regime with bouts of homogeneous firing interrupted by larger synchronous events, $S^{EE} = S^{EI} = S^{IE} = S^{II} = 0.009$ and **c** a more synchronous regime with the majority of the network firing occurring in unison, $S^{EE} = S^{II} = 0.009$, $S^{EI} = S^{IE} = 0.0072$. For all three, the network sizes are $N_E = N_I = 300$, and the Poisson driving parameters are $\eta^E = 550$Hz, $f^E = 0.07$, $\eta^I = 530$Hz, $f^I = 0.07$

Lampl et al. 1999; Lei et al. 2009; Mazzoni et al. 2007; Pertermann 2009; Riffell et al. 2009a, b; Samonds et al. 2005; Yu and Ferster 2010; Yu et al. 2011), but also been revealed in computational studies of the mammalian primary visual cortex (V1) (Cai et al. 2005; Rangan and Young 2012; 2013b), as well as in a number of other computational and analytical studies (Battaglia and Hansel 2011; Benayoun et al. 2010; Brunel and Hakim 1999; Brunel 2000; Cardanobile and Rotter 2010; Hansel and Sompolinsky 1996; Kriener et al. 2008; Renart et al. 2004; Sun et al. 2010; Zhou et al. 2008). The generation of MFEs in idealized spiking neuron networks reflects a strong competition between excitatory and inhibitory populations operating near threshold, providing a possible mechanism underlying similar phenomena observed in real neuronal systems (Anderson et al. 2000; Krukowski and Miller 2000; Murthy and Humphrey 1999; Sillito 1975; Sompolinsky and Shapley 1997; Worgotter and Koch 1991).

The inclusion of MFE dynamics into large-scale computational models has only been possible by carefully resolving each spike (as by Rangan and Cai (2007) for example). Population based methods such as firing rate models and master equations or Fokker-Planck equations rely heavily upon the assumption of the network remaining homogeneous (Brunel and Hakim 1999; Cai et al. 2006; Cai et al. 2004; Rangan and Young 2013a). This assumption is characterized by weak correlations between the individual neurons' evolution, or nearly independent spike times generated across the network (i.e. roughly Poissonian firing statistics). The extension of the master equation to include time correlated MFEs has yet to be fully addressed. The difficulty lies in how to self-consistently incorporate the MFEs into a master equation or Fokker-Planck equation description. Recently, a proposal to circumvent this difficulty computationally has been given in Refs. (Rangan and Young 2013a; Zhang et al. In preparation): stop the evolution of the master equation when an MFE (manifested as a synchronous event of a subset of neurons in the network) occurs, then reshape the population distributions after counting the number of firing neurons participating in the synchronous event, and return to evolving the master equation until next occurrence of an MFE. While the above procedure appears to be straightforward, there are two questions that need to be answered: (1) what is the stopping criteria to indicate that an MFE occurs? and (2) how many neurons participate in an MFE? The first question concerning the stopping criteria depends on the probability of more than two excitatory neurons firing; this question has been addressed by Zhang et al. (In preparation). In this paper, we answer the second question for a specific current-based integrate-and-fire (I&F) neuronal network model by tackling the conceptual issue of how to mathematically characterize MFEs and developing analytical approaches to obtaining the number of neurons firing in an MFE.

In the pulse-coupled current-based integrate-and-fire (I&F) neuronal network model, MFEs are cascade-induced synchronous events occurring at single moments in time; one excitatory neuron fires, increasing the voltages of the other neurons, causing more neurons to fire, and continuing in this cascading fashion until no more neurons fire, or all neurons in the network fire. The independent stochastic processes driving each neuron between synchronous events cause the neuronal voltages to diverge, thus each MFE may include not only a different subset of the population, but may also include entirely different numbers of neurons. Even if all the neurons fire together once, they are not guaranteed to repeat this total synchronous event (see Ref. (Newhall et al. 2010) for a detailed discussion). We are interested in the specific model parameter regime in which the network displays dynamics of substantially sized MFEs separated by time intervals of effectively homogeneous firings. This regime is strongly influenced by the competition between the excitatory and inhibitory populations.

In order to mimic the I&F dynamics using a population-based model, we seek to characterize the MFE by its magnitude, defined as the number of neurons firing together with the neuron(s) initiating the synchronous event, in terms of the information available in the population-based description. Specifically, at the time when the stopping criteria is met (Zhang et al. In preparation), we know the voltage distributions for the excitatory and inhibitory populations, as well as the synaptic coupling strengths and population sizes.

For an all-to-all coupled network of excitatory neurons, the requirement on the individual voltage arrangements for an MFE of a given size to occur was discussed in Ref. (Newhall et al. 2010), but its probability distribution in terms of the voltage distributions could only be computed practically for small MFE sizes. To obtain the size of an MFE, here, we circumvent the "balls-in-bins" combinatorics problem in Ref. (Newhall et al. 2010) by further developing the graphical method presented in Ref. (Rangan and Young 2013a) which is used to describe MFE magnitudes for interacting excitatory and inhibitory populations. We show that the distribution of the MFE size is reducible to the distribution of first passage times of a two-dimensional stochastic process to a moving boundary. While it is possible to write down an explicit partial differential equation for the first passage time distribution of an arbitrary white-noise driven stochastic process to an arbitrary boundary, this equation can only be solved exactly in a very few, simple, cases. In this paper, we approximate the MFE magnitude distribution by extending Durbin's method for 1D passage times with moving boundaries (Durbin and Williams 1992) to the 2D case. The resulting analytical formula for the distribution of MFE magnitudes can not only be easily integrated into population-based methods, but also furnishes a conceptual advantage by illuminating the mechanism underlying MFEs and their dependence on the voltages distributions in different parameter regimes of synaptic strength and population sizes.

The remainder of the paper is organized as follows. In Section 2, we review the Integrate-and-Fire network with inhibitory and excitatory neurons. In Section 3, we develop methods to compute the magnitudes of the MFEs. First, we review the condition for the cascade to continue, and discuss the graphical interpretation of MFEs (see Ref. (Rangan and Young 2013a)), which relates the MFE magnitude to the intersection of a cumulative distribution function (CDF) and a line. Next, we show how to approximate this intersection by replacing the empirical CDF with solutions to two stochastic differential equations, given the original voltage distributions of the excitatory and inhibitory neurons under an appropriate change of variables. Finally, extending Durbin's method, we derive a formula for the density of the first passage time, which in turn provides the magnitude density of MFEs. We finally discuss the validity of our approximations in Section 4 and draw conclusions in Section 5. Many of the mathematical details are described in the Appendixes.

2 Integrate-and-fire network

We consider a model network of all-to-all coupled, current-based I&F neurons consisting of N_E excitatory (E) and N_I inhibitory (I) neurons. The voltage difference across the i^{th} neuron's membrane of type $Q \in \{E, I\}$ obeys the equation

$$\frac{dV_i^Q}{dt} = -g_L\left(V_i^Q - V_L\right) + I_i^{QE} - I_i^{QI} \tag{1a}$$

for $i = 1, \ldots, N_Q$, whenever $V_i^Q < V_T$ for firing threshold V_T and where V_L is the leakage voltage. When the voltage V_i^Q crosses V_T, the neuron is said to generate an action potential; a spike time t_{ik}^Q is recorded and V_i^Q is reset to the reset voltage V_R, and held there for a time τ_{ref}, referred to as the "refractory period". (In all figures we use the non-dimensional values $V_T = 1$ and $V_L = V_R = 0$, see Cai et al. (2005)). The spike times also generate input currents within the last two terms in Eq. (1a). These excitatory and inhibitory currents are given by

$$I_i^{QE} = \sum_l f^Q \delta\left(t - s_{il}^Q\right) + \sum_{j\neq i}\sum_k S^{QE}\delta\left(t - t_{jk}^E\right) \tag{1b}$$

and

$$I_i^{QI} = \sum_{j\neq i}\sum_k S^{QI}\delta(t - t_{jk}^I) \tag{1c}$$

respectively. The first term in the right hand side of Eq. (1b) represents an external driving train of spikes, each with strength f^Q, at the times, s_{il}^Q, generated independently for each neuron from a Poisson point process with rate η^Q. The second term in the right-hand side of Eq. (1b) (the only term in Eq. (1c)) represents the sum over all spikes generated by the excitatory (inhibitory) population of neurons. The current impulse is a delta function; the voltage instantaneously jumps up by an amount f^Q at each external-spike time, S^{QE} at each excitatory-spike time, and decreases by an amount S^{QI} at each inhibitory-spike time.

Equations (1) can be numerically integrated exactly using an event-driven algorithm to determine each of the N_E and N_I neuronal voltages at any instance in time (Brette et al. 2007), together with a procedure to resolve an MFE like the one presented in Appendix A. However, for very large populations, the dynamics (in a homogeneous regime of firing) can be well approximated by the solution to a master equation or a Fokker-Planck equation (Brunel and Hakim 1999; Cai et al. 2004, 2006; Rangan and Young 2013a) for the voltage distributions, $\rho_E(v,t)$ and $\rho_I(v,t)$, of the excitatory and inhibitory populations, respectively. As mentioned previously in the *Introduction* (and shown in (Rangan and Young 2013a; Zhang et al. In preparation)), the master equation or Fokker-Planck equation can be extended to qualitatively capture the feature of MFE dynamics. In the MFE regime, the population has two overall modes which we call the "MFE" mode and the "inter-MFE" mode. In the "inter-MFE" mode, the neurons are weakly correlated or completely independent, and the voltage distribution of neurons can be well described by population equations. When

the criteria for an MFE to occur is satisfied, the inter-MFE mode terminates, and the MFE mode begins. Since the voltages in the corresponding I&F model will instantaneously jump up or down by a synaptic kick, the MFE mode is conceptualized as occurring within a single instant of time. The non-zero refractory period will ensure that a neuron only fires once during an MFE. From the available voltage distributions, $\rho_E(v,t)$ and $\rho_I(v,t)$, it is important to have an efficient method for determining the MFE magnitude and therefore effectively capture the features of the MFE regime.

The focus of this paper is developing different approaches to obtain the size of an MFE during the MFE mode. Incidentally, in what follows, we do not present the details of the master equation, but assume we have access to $\rho_E(v)$ and $\rho_I(v)$, the distributions of neuronal voltages at the time some excitatory neurons are about to fire and trigger an MFE.

3 Determining MFE magnitude

As mentioned in the *Introduction*, many biologically realistic regimes include bursts of firing activity similar in nature to MFEs. Due to the delta function impulses, the network modeled by Eq. (1) can exhibit MFEs in the form of cascade-induced synchrony (Newhall et al. 2010), in which the external driving causes one excitatory neuron to spike, instantaneously increasing the voltages of other neurons, causing more excitatory (and possibly inhibitory) neurons to fire, increasing (and possibly decreasing) the voltages of other neurons, cascading through the network, resulting in many neurons spiking at the exact same instant time. The number of neurons participating in one such MFE is determined solely by the arrangement of all the voltages at the time one excitatory neuron fires, as well as by the four coupling strengths, S^{EE}, S^{IE}, S^{EI} and S^{II}. We therefore seek the connection between the voltage distributions of the excitatory and inhibitory populations at the time when the MFE is initiated, and the distribution of MFE magnitudes (number of spiking excitatory and inhibitory neurons in one such event). In this section, we achieve this by calculating the distribution of MFE magnitudes in three ways: In Section 3.1 we present the condition for the cascading firing event to continue in terms of the set of excitatory $\{v_j\}_{j=1}^{N_E}$ and inhibitory $\{w_j\}_{j=1}^{N_I}$ neuronal voltages at the time one excitatory neuron is about to fire, and compute the MFE magnitude graphically from the intersection of a line and a function of the empirical voltage CDFs. In Section 3.2 we approximate the empirical CDF by a stochastic process depending on the voltage density distributions (not the set of voltages themselves) and calculate the MFE magnitude as a first passage time problem. Finally, in Section 3.3 we approximate the solution to the first passage time problem and obtain the distribution of MFE magnitudes in terms of the voltage distributions, numbers of neurons, and the coupling strengths.

3.1 Geometrical method

We will begin by describing the connection between the cascade-mechanism responsible for an MFE and a graphical representation of its magnitude. The connection is easiest to understand if we consider only a population of excitatory neurons with a set of sorted descending voltages, $\{v^{(j)}\}_{j=1}^{N_E}$ with $v^{(j)} \geq v^{(i)}$ for $j < i$, at the time one neuron fires ($v^{(1)} \geq V_T$). The MFE will continue with a second neuron firing if $v^{(2)} \in \left[V_T - S^{EE}, V_T\right)$, as all neuronal voltages are increased by S^{EE} when the neuron with voltage $v^{(1)}$ fires. A third neuron will fire if $v^{(3)} \in \left[V_T - 2S^{EE}, V_T\right)$, the two previously firing neurons cause the voltages of remaining neurons to increase by $2S^{EE}$. Exactly m_E neurons will fire if the condition

$$v^{(j)} \in \left[V_T - (j-1)S^{EE}, V_T\right) \tag{2}$$

is satisfied for $j = 2 \ldots m_E$ but not for $j = m_E + 1$. If we define the empirical CDF to be

$$F_E(v) = \int_{-\infty}^{v} \frac{1}{N_E} \sum_{j=1}^{N_E} \delta(z - v_j) dz, \tag{3}$$

then satisfying condition (2) for $j = 1$ to m_E is equivalent to satisfying the condition

$$V_T - v \leq S^{EE} N_E (1 - F_E(v)) \tag{4}$$

for $v < V_T$ such that $N_E(1 - F_E(v)) \leq m_E$. The magnitude, m_E, can be determined by the value V^* for which condition (4) is no longer true. This is precisely the point V^* where the CDF $F_E(v)$ intersects the line

$$l(v) = 1 + \frac{1}{N_E S^{EE}}(v - V_T). \tag{5}$$

The MFE magnitude is then given by

$$m_E = N_E \left[1 - F_E(V^*)\right].$$

Figure 2 demonstrates this graphical interpretation. As the voltage configuration before the MFE changes, the empirical CDF $F_E(v)$ will also change, as will the intersection point, V^* and hence the MFE magnitude, m_E. Because the underlying distribution for the excitatory voltages can be multi-modal, (c.f. Fig. 2c), it is possible for V^* to be discontinuous as a function of S^{EE}.

We extend the above geometrical method to account for the addition of an inhibitory population of neurons with

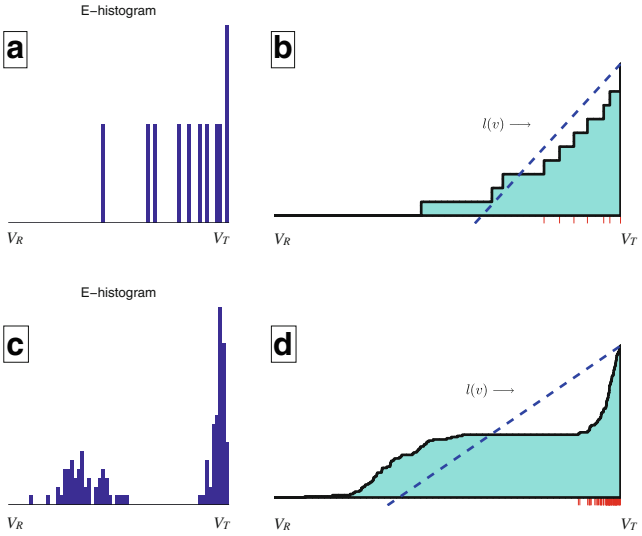

Fig. 2 Geometrical method for determining the MFE magnitudes in a population of excitatory neurons. **a** The histogram of $N_E = 10$ excitatory neurons when one is about to fire. **b** The intersection of the empirical CDF $F_E(v)$ (*black line over cyan shaded region*) and the line $l(v) = 1 + \frac{1}{N_E S^{EE}}(v - V_T)$ (blue dashed line) is the point when the cascading MFE terminates: for voltages above this point there are $j = 7$ neurons within the interval $\left[V_T - jS^{EE}, V_T\right]$ with $S^{EE} = 0.04$, and these neurons will fire in the MFE. Below this point, condition (2) is violated. The *red* ticks on the x-axis indicate the voltages of the neurons firing in the MFE. (**c** and **d**) Same as (**a** and **b**) but for a bimodal distribution of voltages, $N_E = 128$, and $S^{EE} = 0.005$

voltages $\left\{w_j\right\}_{j=1}^{N_I}$ and empirical CDF

$$F_I(w) = \int_{-\infty}^{w} \frac{1}{N_I} \sum_{j=1}^{N_I} \delta(z - w_j) dz.$$

Inhibitory neurons impede the continuation of MFEs as each generated spike reduces the excitatory voltages by S^{EI} and the other inhibitory voltages by S^{II}. Therefore, the analogous condition to Eq. (4) for the cascade to continue when there are two populations is

$$\begin{aligned} V_T - v &\le S^{EE} N_E \left(1 - F_E(v)\right) - S^{EI} N_I (1 - F_I(w)), \\ V_T - w &\le S^{IE} N_E \left(1 - F_E(v)\right) - S^{II} N_I (1 - F_I(w)). \end{aligned} \tag{6}$$

The magnitude of the MFE is found from the points $v = V^*$ and $w = W^*$ such that for $v < V^*$ and $w < W^*$ the conditions in Eq. (6) no longer hold. What we do next is describe how to reduce the failure of the two conditions in Eq. (6) as the intersection of a function of only v and the line in Eq. (5), thereby deriving the MFE magnitude in terms of a single intersection point as was just done for only the excitatory population. We present a simple overview here; the details are explained in Appendix B.

We first rescale the inhibitory voltages to

$$\hat{w}_j = V_T - \frac{S^{EE}}{S^{IE}} \left(V_T - w_j\right), \tag{7}$$

so that the firing of one excitatory neuron will cause an inhibitory neurons to fire if its rescaled voltage $\hat{w}_j$ is in the interval $\left[V_T - S^{EE}, V_T\right]$. This allows the difference between the two conditions in Eq. (6) to be written as the single condition appearing in Eq. (44) in Appendix B. We also define the empirical inhibitory voltage CDF,

$$\hat{F}_I(w) = \lim_{V \to w^-} \int_{-\infty}^{V} \frac{1}{N_I} \sum_{j=1}^{N_I} \delta\left(z - \hat{w}_j\right) dz, \tag{8}$$

associated with the transformed voltages in Eq. (7). Next, we have two cases: If the inhibitory effect on the inhibitory neurons is larger than on the excitatory neurons, i.e., $\delta = S^{II} S^{EE} / S^{IE} - S^{EI} > 0$, then we need to shift $\hat{w}_j$ further by defining

$$\bar{v}_j = v_j, \quad \bar{w}_j = \hat{w}_j - \delta N_I \left(1 - \hat{F}_I\left(\hat{w}_j\right)\right). \tag{9}$$

On the other hand, if the inhibitory effect on the excitatory neurons is larger than the inhibitory neurons, i.e., $\delta = S^{II} S^{EE} / S^{IE} - S^{EI} < 0$, then we shift the v_j by

$$\bar{v}_j = v_j + \delta N_I \left(1 - \hat{F}_I\left(\bar{v}_j\right)\right), \quad \bar{w}_j = \hat{w}_j. \tag{10}$$

By constructing new CDFs for the transformed variables,

$$\begin{aligned} \bar{F}_E(v) &= \int_{-\infty}^{v} \frac{1}{N_E} \sum_{j=1}^{N_E} \delta\left(z - \bar{v}_j\right) dz, \\ \bar{F}_I(v) &= \int_{-\infty}^{v} \frac{1}{N_I} \sum_{j=1}^{N_I} \delta\left(z - \bar{w}_j\right) dz, \end{aligned} \tag{11}$$

we have that

$$\frac{V_T - \bar{v}}{N_E S^{EE}} \le 1 - \bar{F}_E(\bar{v}) - \alpha \left(1 - \bar{F}_I\left(\bar{v}\right)\right) \tag{12}$$

is equivalent to the two conditions in Eq. (6). The value $\alpha = \min\left(\frac{S^{II}}{S^{IE}}, \frac{S^{EI}}{S^{EE}}\right) \frac{N_I}{N_E}$ is obtained by considering that $\delta \ge 0$ implies $\frac{S^{II}}{S^{IE}} > \frac{S^{EI}}{S^{EE}}$, and $\delta < 0$ implies $\frac{S^{II}}{S^{IE}} < \frac{S^{EI}}{S^{EE}}$. Condition (12) is equivalent to the conditions (50) and (56) derived in Appendix B for the two different cases of δ.

Interpreting condition (12) failing for the first time as an intersection point, we determine the magnitude of the MFE as

$$m_Q = N_Q \left[1 - \bar{F}_Q\left(V^*\right)\right], \tag{13}$$

where V^* is the intersection point of the new function

$$G(v) = \bar{F}_E(v) + \alpha \left[1 - \bar{F}_I(v)\right], \tag{14}$$

and the line $l(v)$ in Eq. (5). Notice that each initial set of specific voltages $\left\{v_j\right\}_{j=1}^{N_E}$ and $\left\{w_j\right\}_{j=1}^{N_I}$ yields exactly one MFE

magnitude. We can obtain the distribution of MFE magnitudes by repeated sampling of the sets of voltages $\{v_j\}_{j=1}^{N_E}$ and $\{w_j\}_{j=1}^{N_I}$ from some known densities $\rho_E(v)$ and $\rho_I(w)$, respectively, and computing the MFE magnitude using the above algorithm.

3.2 First passage time formulation

Having derived a method above for obtaining the magnitude of an MFE in terms of the empirical CDFs of the excitatory and inhibitory populations, we are now ready to reformulate the problem of obtaining the magnitude of an MFE as a first passage time problem. We take advantage of Donsker's theorem (Donsker 1952) to approximate the empirical CDFs in terms of rescaled Brownian Bridges.[1] In this framework, in which "time" is considered the voltage difference from the threshold voltage V_T, the intersection point of interest, and thus the MFE magnitude, is the first passage time of a stochastic process to a line.

Here, we first derive the theoretical CDFs for the transformed voltages $\bar{v}_j$ and $\bar{w}_j$ defined in the previous section in terms of "time" starting from the original probability density functions (PDFs) for the voltages of the excitatory and inhibitory populations. (Recall from the end of Section 2 we assume that we have access to these distributions at the time an excitatory neuron fires.) Then, from the theoretical PDFs we can write two stochastic differential equations (SDEs) that approximate the possible empirical CDFs. We obtain the MFE magnitude by simulating the SDEs and determining the first passage time. In the next section, we complete the connection between the population voltage distributions and the distribution of MFE magnitudes by analytically approximating the first passage time density.

First, in the framework of time defined as $t = V_T - v$, we derive the theoretical PDFs for the transformed voltages defined in either Eq. (9) or Eq. (10), starting from the original theoretical PDFs for the excitatory and inhibitory voltages, $\rho_E(v)$ and $\rho_I(w)$, respectively. Switching to t and using the transformation in Eq. (7), we obtain the transformed PDFs $p_E(s) = \rho_E(V_T - s)$ and $p_I\left(\hat{t}\right) = \frac{S^{IE}}{S^{EE}}\rho_I\left(V_T - \frac{S^{IE}}{S^{EE}}\hat{t}\right)$. The equivalent formulas to Eqs. (9) and (10) for transforming the variables s and $\hat{t}$ are

$$\bar{s} = s, \qquad \bar{t} = \hat{t} + \delta N_I \hat{f}_I\left(\hat{t}\right), \qquad \text{if } \delta \geq 0, \tag{15a}$$

$$\bar{s} = s - \delta N_I \hat{f}_I\left(\bar{s}\right), \qquad \bar{t} = \hat{t}, \qquad \text{if } \delta < 0, \tag{15b}$$

[1] Donsker's theorem states that the fluctuations of an empirical CDF about its theoretical CDF converge to Gaussian random variables with zero mean and certain variance. The sequence of independent Gaussian random variables can be formulated in terms of a standard Brownian bridge, a continuous-time stochastic process on the unit interval, conditioned to begin and end at zero.

where $\delta = S^{II}S^{EE}/S^{IE} - S^{EI}$ as before and where we have defined $\hat{f}_I(t) = \int_0^t p_I(\tau)d\tau$.

We now consider the densities for these new variables $\bar{s}$ and $\bar{t}$ for two cases. First, if $\delta \geq 0$, then we can approximate the distributions of $\bar{t}$ and $\bar{s}$ as

$$\bar{p}_I\left(\bar{t}\right) = \frac{p_I\left(g^{-1}\left(\bar{t}\right)\right)}{g'\left(g^{-1}\left(\bar{t}\right)\right)} \quad \text{and} \quad \bar{p}_E(\bar{s}) = p_E(\bar{s}) \tag{16}$$

where we have defined $g(t) = t + \delta N_I \hat{f}_I(t)$, and $g'(t)$ is the derivative with respect to t. Similarly, for the case when $\delta < 0$,

$$\bar{p}_E(\bar{s}) = p_E(g(\bar{s}))g'(\bar{s}) \quad \text{and} \quad \bar{p}_I(\bar{t}) = p_I(\bar{t}). \tag{17}$$

Finally, we define the theoretical CDFs of these transformed densities by

$$\bar{f}_E(t) = \int_0^t \bar{p}_E(\tau)d\tau \quad \text{and} \quad \bar{f}_I(t) = \int_0^t \bar{p}_E(\tau)d\tau. \tag{18}$$

One example of transforming the PDFs is shown in Fig. 3. The original PDFs $\rho_E(v)$ and $\rho_I(w)$ are shown in Fig. 3a while the transformed PDFs in Eq. (16) are shown in Fig. 3b for one choice of coupling strengths.

What we have so far is a way to transform from the PDFs of the excitatory and inhibitory population voltages to the theoretical CDFs of the transformed voltages. Note that the MFE is determined by the intersection of a combination of the *empirical* CDFs and the line in Eq. (5). We now use Donsker's Theorem (Donsker 1952) to approximate the possible empirical distributions, $\tilde{F}_Q(t)$, selected at random from the theoretical distributions in Eq. (18), as

$$\tilde{F}_Q(t) \approx \bar{f}_Q(t) + \frac{1}{\sqrt{N_Q}} B\left(\bar{f}_Q(t)\right) \tag{19}$$

for $Q \in \{E, I\}$, where $B(\cdot)$ is a standard Brownian bridge on the unit interval starting and ending at zero. The approximation (19) will be valid when $N_E, N_I \gg 1$. A single stochastic trajectory, $\phi_Q(t) = \frac{1}{\sqrt{N_Q}} B\left(\bar{f}_Q(t)\right)$, solves the stochastic differential equation

$$d\phi_Q(t) = -\frac{\phi_Q(t)\bar{p}_Q(t)}{1 - \bar{f}_Q(t)}dt + \sqrt{\frac{\bar{p}_Q(t)}{N_Q}}dW_Q(t) \tag{20}$$

with $\phi_Q(0) = 0$, and where $dW_Q(t)$ is standard white noise in time.

We must also know how many neurons initiate the MFE, as the population-based description does not include any neurons with voltages over the threshold. If precisely k excitatory neurons fire to initiate the MFE, then the MFE magnitudes are derived from the first intersection point of

$$\bar{G}(t) = \gamma(\bar{f}_E(t) + \phi_E(t)) - \alpha(\bar{f}_I(t) + \phi_I(t)) + \frac{k}{N_E} \tag{21}$$

with the line

$$\bar{l}(t) = \frac{1}{N_E S^{EE}} t, \tag{22}$$

where $\gamma = 1 - k/N_E$ and $\alpha = \min\left(\frac{S^{II}}{S^{IE}}, \frac{S^{EI}}{S^{EE}}\right)\frac{N_I}{N_E}$, as before. Note that $\bar{G}(t)$ is different from the direct transformation of $G(v)$ (Eq. 14) to either set of variables defined in Eq. (15) in that $\bar{G}(t)$ also takes into account the k excitatory neurons that initiate the MFE.

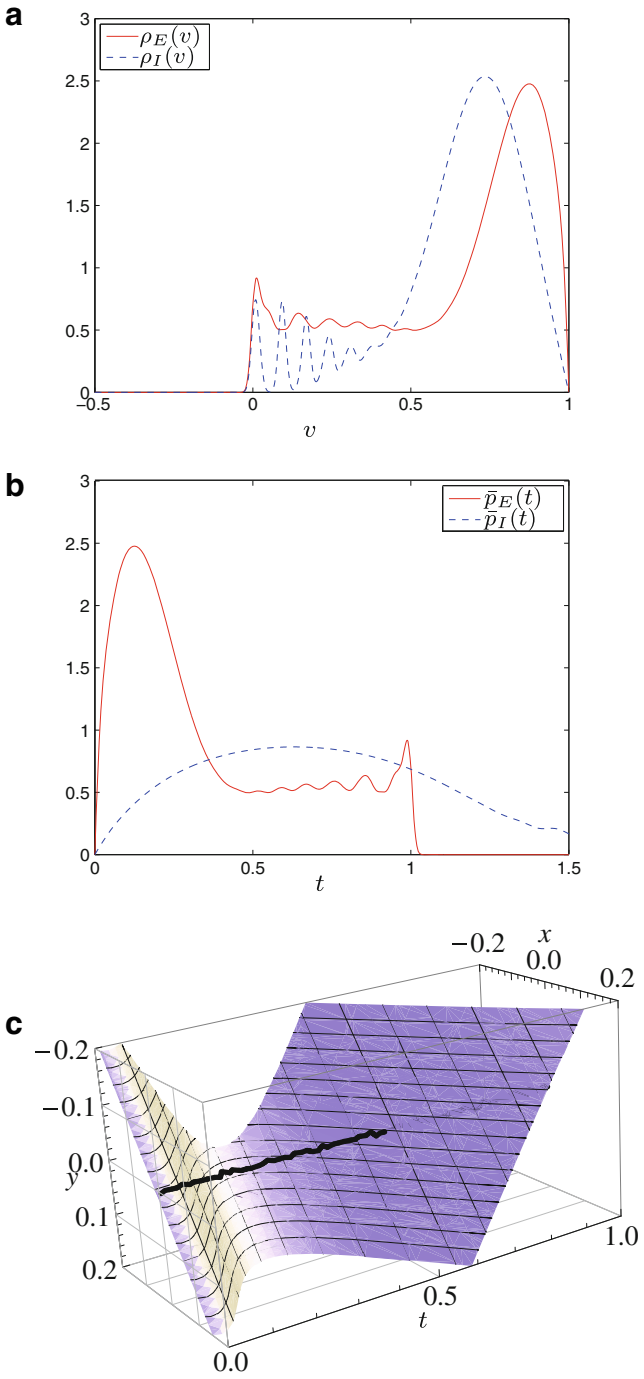

Fig. 3 **a** The original densities $\rho_E(v)$ and $\rho_I(v)$. **b** The transformed densities $\bar{p}_E(t)$ and $\bar{p}_I(t)$ defined in Eq. (16) for the case when $S^{EE} = 0.009$, $S^{IE} = 0.0072$, $S^{EI} = 0.0057$, $S^{II} = 0.0072$ and $N_E = N_I = 128$. **c** A sample trajectory of the SDE (*black line*) for the densities shown in (**b**) intersecting the surface $\mathcal{A}$ in the 3D space (x, y, t)

Finally, we determine the magnitudes of the MFE by finding the first point in time when $\bar{G}(t)$ in Eq. (21) crosses the line $\bar{l}(t)$ in Eq. (22), or equivalently in three-dimensional space, the first time, t^*, that the joint stochastic process $(\phi_E(t), \phi_I(t), t)$ exits the region bounded by the surface $\mathcal{A}$ given by the algebraic constraint that $\bar{G}(t) = \bar{l}(t)$ for points (x, y, t):

$$-\gamma(x + \bar{f}_E(t)) + \alpha(y + \bar{f}_I(t)) + \frac{1}{N_E S^{EE}} t = \frac{k}{N_E}. \quad (23)$$

Figure 3c shows an example trajectory crossing this surface. Given this intersection point, t^*, the magnitudes of the MFE are

$$\begin{aligned} m_E &= k + [N_E - k]\left(\bar{f}_E(t^*) + \phi_E(t^*)\right), \\ m_I &= N_I\left(\bar{f}_I(t^*) + \phi_I(t^*)\right). \end{aligned} \quad (24)$$

Using the above formulation, we can numerically determine the distribution of MFE magnitudes as follows: First, take the theoretical PDFs $\rho_E(v)$ and $\rho_I(w)$ and transform them to $\bar{p}_E(t)$ and $\bar{p}_I(t)$ using either Eq. (16) or Eq. (17) and then calculate the CDFs $\bar{f}_E(t)$ and $\bar{f}_I(t)$ defined in Eq. (18). Next, using these transformed PDFs and CDFs, simulate stochastic trajectories using Eq. (20), and determine the intersection point of $(\phi_E(t), \phi_I(t), t)$ with the surface $\mathcal{A}$ in Eq. (23). Last, compute the MFE magnitudes in Eq. (24). The distribution of MFE magnitudes is obtained by repeatedly simulating the stochastic trajectories and determining the intersection points. Next, in Section 3.3, we devote ourselves to deriving an analytical formula for this MFE magnitude distribution.

3.3 Analytical formula for the distribution of MFE magnitudes

In Section 3.2, we reduced the problem of obtaining the MFE magnitude to one of finding the first exit time (or first passage time) of the joint stochastic process $(\phi_E(t), \phi_I(t), t)$ out of the region bounded by the surface $\mathcal{A}$. This can also be thought of as a 2D stochastic process $(\phi_E(t), \phi_I(t))$ hitting a moving boundary. Durbin's method of approximating first passage time distributions of 1D stochastic trajectories to moving boundaries (Durbin 1985; Durbin and Williams 1992) depends on the distance between the surface and the starting point of the trajectory and the distribution of the stochastic trajectory as a function of time. We employ a similar technique by first transforming the 2D stochastic process to an isotropic 2D stochastic process with the same diffusion in any direction. This allows us to decompose the process into the directions perpendicular and parallel to the surface $\mathcal{A}$. The problem reduces to a 1D passage time of the perpendicular component to the

boundary. Here, we briefly describe how to obtain the two term approximation of this first passage time density; details appear in Appendix C.

We begin by conditioning on some additional information to determine the first passage time density $p_T(t)$ of the process $(\phi_E(t), \phi_I(t), t)$ to the surface $\mathcal{A}$ in Eq. (23). First we include the location $\mathbf{a} = (a_E, a_I)$ on the boundary that the process hits, and write $p_T(t)$ in terms of the joint distribution $p(t, \mathbf{a})$ for first hitting the point $\mathbf{a}$ at time t as

$$p_T(t) = \int_{\mathcal{A}|_t} p(t, \mathbf{a}) d\mathbf{a}, \tag{25}$$

where the integration is over $\mathcal{A}|_t$, i.e., all points on the surface at time t. Then, we condition on the process being at the point $\mathbf{x}$ at some intermediate time s. In order to have a first passage time t and hit $\mathbf{a}$, the trajectory must first get to $\mathbf{x}$ at time s without hitting the boundary $\mathcal{A}$ and then proceed to have a first passage time t to the point $\mathbf{a}$. In terms of distributions, we may write

$$p(t, \mathbf{a}) = \int_{\Omega(s)} p(t, \mathbf{a}|s, \mathbf{x}) g(s, \mathbf{x}) d\mathbf{x}, \tag{26}$$

where $p(t, \mathbf{a}|s, \mathbf{x})$ is the first passage time density to $\mathbf{a}$ at time t given the trajectory starts at the point $\mathbf{x}$ at time s, $g(s, \mathbf{x})$ is the density of the process at $\mathbf{x}$ at time s given that it did not cross $\mathcal{A}$ previously, and the integration is over $\Omega(s)$. $\Omega(s)$ represents all points at time s in the (x, y) plane with the boundary $\partial\Omega = \mathcal{A}$.

To derive an expression for $p(t, \mathbf{a}|s, \mathbf{x})$ we consider two independent processes: one moves perpendicular to the boundary $\mathcal{A}$ which controls the time the boundary is hit, and one moves parallel to the boundary which controls at which point the boundary is hit. This is possible if we consider s sufficiently close to t (i.e., $t - s \ll 1$). Over the small time interval $[s, t]$ we approximate the joint process (ϕ_E, ϕ_I) by two component Brownian motion, $\left(\hat{\phi}_E, \hat{\phi}_I\right)$ (constant drift and diffusion coefficients) that solves Eq. (20) with frozen coefficients at time s, and consider hitting the boundary, $\hat{\mathcal{A}}_{a(t)}$. $\hat{\mathcal{A}}_{a(t)}$ is a plane tangent to the surface $\mathcal{A}$ at the point $\mathbf{a}$ at time t. To decompose $\left(\hat{\phi}_E, \hat{\phi}_I\right)$ into *independent* parallel and perpendicular to $\hat{\mathcal{A}}_{a(t)}$ components, we must first transform it into isotropic Brownian motion (same diffusion in all directions) with the transformation matrix

$$\beta = \begin{pmatrix} \sqrt{\frac{\bar{p}_E(s)}{N_E}} & 0 \\ 0 & \sqrt{\frac{\bar{p}_I(s)}{N_I}} \end{pmatrix},$$

and then decompose it into the directions perpendicular to $\hat{\mathcal{A}}_{a(t)}$ given by vector

$$n_\perp = \frac{1}{\eta}[-\gamma, \alpha]$$

and parallel to $\hat{\mathcal{A}}_{a(t)}$ given by vector

$$n_\parallel = \frac{1}{\eta}[\alpha, \gamma],$$

where

$$\eta = \left[-\gamma, \alpha, \alpha \bar{p}_I(t) - \gamma \bar{p}_E(t) + \frac{1}{N_E S^{EE}}\right] \tag{27}$$

is the three component normal of $\hat{\mathcal{A}}_{a(t)}$. Now, we approximate $p(t, \mathbf{a}|s, \mathbf{x})$ as

$$p(t, \mathbf{a}|s, \mathbf{x}) \approx f(t, \mathbf{a}|s, \mathbf{x}) \times \frac{\widehat{\mathcal{A}}_{a(t)}|_s - \mathbf{x}}{t - s} \cdot n_\perp \frac{\left|\beta^{-1} n_\parallel\right|}{|\beta n_\perp|} \frac{|\beta|}{|n_\perp| \left|n_\parallel\right|}, \tag{28}$$

following Durbin by adjusting the density, $f(t, \mathbf{a}|s, \mathbf{x})$, of the process starting at $\mathbf{x}$ at time s to be at the boundary point $\mathbf{a}$ at time t by the probability for the parallel component of the isotropic Brownian motion to hit the boundary and the probability for the perpendicular component to reach the point $\mathbf{a}$. In (28) $\widehat{\mathcal{A}}_{a(t)}|_s$ are points on the tangent boundary $\hat{\mathcal{A}}_{a(t)}$ at the time s. Using approximation (28) in the limit as $s \to t$, Eq. (26) remains exact and can be expressed as

$$p(t, \mathbf{a}) = \lim_{s \to t^-} \frac{f(t, \mathbf{a})}{t - s} \times \int_{\partial\Omega(s)} \left(\widehat{\mathcal{A}}_{a(t)}|_s - \mathbf{x}\right) \cdot \mathbf{u}\zeta(t) g(s, \mathbf{x}) d\mathbf{x}, \tag{29}$$

where we have defined $\mathbf{u} = [-\gamma, \alpha]/\sqrt{\gamma^2 + \alpha^2}$, and $\zeta(t) = \sqrt{1 + 1/\nu_n^2(t)}$ so that

$$\mathbf{u}\zeta(t) = n_\perp \frac{\left|\beta^{-1} n_\parallel\right|}{|\beta n_\perp|} \frac{|\beta|}{|n_\perp| \left|n_\parallel\right|}$$

and the quantity

$$\nu_n(t) = \frac{\sqrt{\gamma^2 + \alpha^2}}{\alpha \bar{p}_I(t) - \gamma \bar{p}_E(t) + 1/\left(N_E S^{EE}\right)} \tag{30}$$

can be thought of as the speed at which the boundary propagates in the normal direction.

So far, we have described how to obtain $p(t, \mathbf{a})$ in Eq. (29) as an adjustment to the density $f(t, \mathbf{a})$, for the process at $(t, \mathbf{a})$. By writing Eq. (29) as

$$\begin{aligned} p(t, \mathbf{a}) = & \lim_{s \to t^-} \frac{f(t, \mathbf{a})}{t - s} \mathbb{E}\left[\left(\widehat{\mathcal{A}}_{a(t)}|_s - \mathbf{x}\right) \cdot \mathbf{u}\zeta(t) | \text{cross } (t, \mathbf{a})\right] \\ & - \lim_{s \to t^-} \frac{f(t, \mathbf{a})}{t - s} \mathbb{E}\Big[\left(\widehat{\mathcal{A}}_{a(t)}|_s - \mathbf{x}\right) \cdot \mathbf{u}\zeta(t) | \text{cross } (t, \mathbf{a}), \\ & \qquad \text{first crossing } (r, \mathbf{b}), \\ & \qquad \text{where } r < t\Big] \end{aligned} \tag{31}$$

and defining $q(t, \mathbf{a}) = p(t, \mathbf{a})/f(t, \mathbf{a})$ we arrive at an integral equation for $q(t, \mathbf{a})$. We approximate its solution with two terms and obtain

$$p(t, \mathbf{a}) \approx (q_0(t, \mathbf{a}) - q_1(t, \mathbf{a}))\, f(t, \mathbf{a}), \tag{32}$$

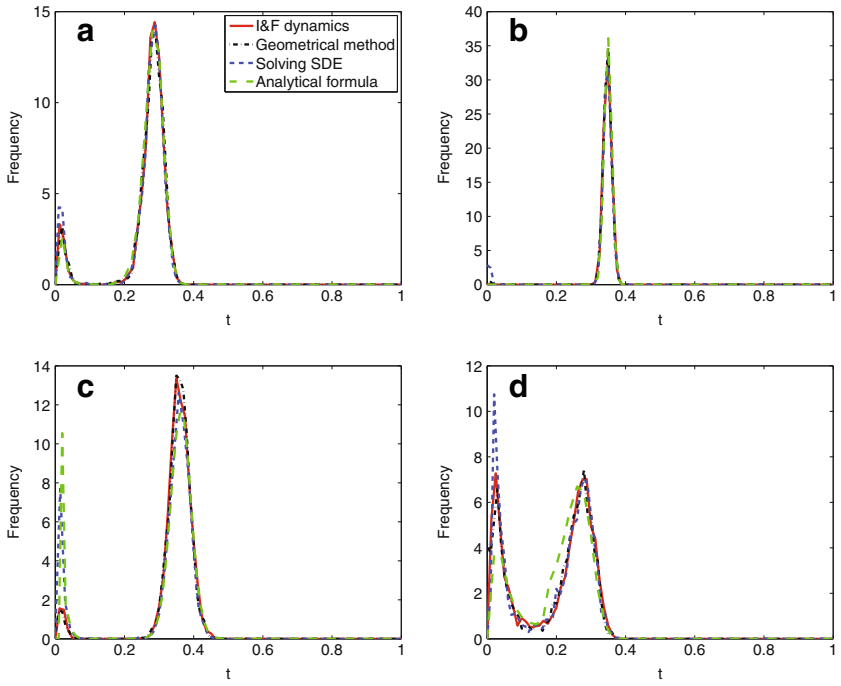

Fig. 4 Distribution of the intersection point t for the three methods in Section 3 starting from the same voltage distributions, $\rho_E(v)$ and $\rho_I(v)$ shown in Fig. 3**a**, and initiated by $k = 2$ neurons (the excitatory and inhibitory MFE magnitudes are given in Eq. (35) in terms of t^*, a value selected from the shown distribution). **a** $S^{EE} = S^{II} = S^{IE} = S^{EI} = 0.009$, and $N_E = N_I = 300$, **b** $S^{EE} = S^{II} = S^{IE} = S^{EI} = 0.008$, and $N_E = N_I = 2000$, **c** $S^{EE} = S^{IE} = 0.009$, $S^{II} = S^{EI} = 0.0072$, $N_E = N_I = 300$, and (**d**) $S^{EE} = 0.009$, $S^{II} = 0.0072$, $S^{IE} = S^{EI} = 0.0081$, $N_E = N_I = 128$

for the density of the first passage time to the point $\mathbf{a}(t) = (a_E(t), a_I(t))$ on the surface $\mathcal{A}$, with

$$q_0(t,\mathbf{a}) = \left(\sqrt{1+\nu_n^2(t)} - \frac{\zeta(t)}{\sqrt{\gamma^2+\alpha^2}} \times \left[\alpha\frac{a_I(t)\bar{p}_I(t)}{\bar{f}_I(t)} - \gamma\frac{a_E(t)\bar{p}_E(t)}{\bar{f}_E(t)}\right]\right)$$

and with

$$q_1(t,\mathbf{a}) = \int_0^t \int_{\partial\Omega(r)} q_0(r,\mathbf{b}) f(r,\mathbf{b}|t,\mathbf{a}) \times \left(-\sqrt{1+\nu_n^2(t)} + \left[\alpha\frac{(a_I(t)-b_I(r))\,\bar{p}_I(t)}{\bar{f}_I(t)-\bar{f}_I(r)} - \gamma\frac{(a_E(t)-b_E(r))\,\bar{p}_E(t)}{\bar{f}_E(t)-\bar{f}_E(r)}\right]\frac{\zeta(t)}{\sqrt{\gamma^2+\alpha^2}}\right) d\mathbf{b}dr,$$

where $\nu_n(t)$ is given in Eq. (30), $\alpha = \frac{N_I}{N_E}\min\left\{\frac{S^{II}}{S^{IE}}, \frac{S^{EI}}{S^{EE}}\right\}$ and $\gamma = 1 - k/N_E$ as before. The point $\mathbf{b}(r) = (b_E(r), b_I(r))$ is another point on the surface $\partial\Omega = \mathcal{A}$ at time $r \le t$, i.e., both $\mathbf{a}(t)$ and $\mathbf{b}(r)$ satisfy the condition to lie on the surface given in Eq. (23).The density of the process at point $\mathbf{a}$ at time t is

$$f(t,\mathbf{a}) = \frac{1}{2\pi\sqrt{\sigma_E(t)\sigma_I(t)}}\exp\left(-\frac{a_E^2(t)}{2\sigma_E(t)} - \frac{a_I^2(t)}{2\sigma_I(t)}\right) \tag{33}$$

where $\sigma_E(t) = \bar{f}_E(t)\left(1-\bar{f}_E(t)\right)/(N_E-k)$ and $\sigma_I(t) = \bar{f}_I(t)\left(1-\bar{f}_I(t)\right)/N_I$ and the density of process at the point $\mathbf{a}$ at time t given that it was previously at the point $\mathbf{b}$ at time r and did not cross the surface $\mathcal{A}$ before time r is

$$f(r,\mathbf{b}|t,\mathbf{a}) = \frac{\bar{f}_E(t)\bar{f}_I(t)}{2\pi\sqrt{\sigma_E(r,t)\sigma_I(r,t)}} \times \exp\left(-\frac{\left[b_E\bar{f}_E(t) - a_E\bar{f}_E(r)\right]^2}{2\sigma_E(r,t)} - \frac{\left[b_I\bar{f}_I(t) - a_I\bar{f}_I(r)\right]^2}{2\sigma_I(r,t)}\right) \tag{34}$$

where $\sigma_E(r,t) = \bar{f}_E(r)(\bar{f}_E(t) - \bar{f}_E(r))/(N_E-k)$ and $\sigma_I(r,t) = \bar{f}_I(r)(\bar{f}_I(t) - \bar{f}_I(r))/N_I$. These two distributions are derived in Appendix D.

Recall that these formulas all involve the densities of the transformed variables $\bar{s}$ and $\bar{t}$ defined in Section 3.2. From the original voltage densities, $\rho_E(v)$ and $\rho_I(v)$ at the time the MFE is initiated, the transformed PDFs $\bar{\rho}_Q(t)$ must be calculated using Eq. (16) if $\delta \ge 0$ (recall $\delta = S^{II}S^{EE}/S^{IE} - S^{EI}$) or Eq. (17) if $\delta < 0$, then the transformed CDFs $\bar{f}_Q(t)$ calculated from Eq. (18). The final step is to select t^* from Eq. (25) with $p(t,\mathbf{a})$ approximated by Eq. (32) and compute the MFE magnitudes using

$$\begin{aligned} m_E &= k + (N_E - k)\left(a_E^* + \bar{f}_E(t^*)\right) \\ m_I &= N_I\bar{f}_I(t^*), \end{aligned} \tag{35}$$

where a_E^* is drawing from the density $p(t^*,\mathbf{a})$ after fixing t^*.

The MFE magnitude density is computed by selecting many values of t^* from the distribution in Eq. (25) and then determining the magnitude of the MFE from Eq. (35). As we discuss in the next section, the density computed in this

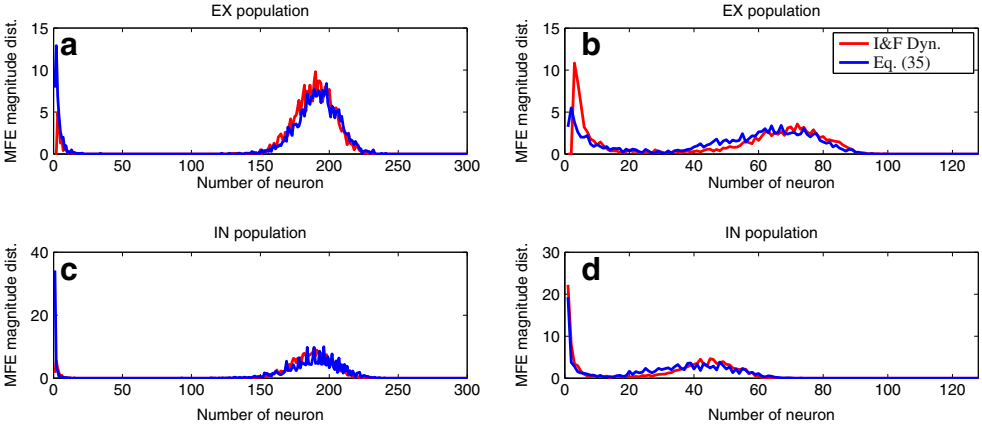

Fig. 5 Distribution of MFE magnitudes computed by resolving the I&F dynamics as in Ref. (Rangan and Young 2013a), and by selecting random times from the distribution in Eq. (25) to use in Eq. (35) for the same two cases shown in Fig. 4**c** and **d**: *Left* corresponds to Fig. 4**c** and *right* corresponds to Fig. 4**d**. The panels show the distributions of MFE magnitudes for the excitatory population (*upper graph*) and for the inhibitory population (*lower graph*), respectively

manner is in excellent agreement with the density computed using an appropriate method for the original I&F dynamics, such as the one presented in Appendix A or the one by Rangan and Young (2013a).

4 Validity of approximations

In Section 3 we discussed three methods for determining the density of MFE magnitudes in term of the original voltage densities of the excitatory and inhibitory neurons. We now discuss the error introduced in each method, and present the numerically obtained distributions in order to examine the propagation of the error through the entire procedure. In the end, we find excellent agreement between the distribution obtained by using the I&F dynamics (as described by Rangan and Young (2013a)) and the single formula (25) obtained in Section 3.3.

First, we point out that resolving an MFE with I&F dynamics is indistinguishable from resolving it with the geometric method using the true empirical CDFs in Section 3.1 when using the same set of voltages. Their respective distributions will only vary from the true MFE distribution due to statical error. This can be seen in Fig. 4, where the MFE magnitude distribution is shown in terms of the intersection point in the transformed variable t. The red solid line corresponding to the intersection points obtained from the I&F dynamics is nearly indistinguishable from the black dot-dash line corresponding to the geometrically obtained intersection points in all four parameter cases.

The first approximation occurs in Section 3.2 when the empirical CDFs are replaced by approximations constructed by adding white noise driven stochastic processes to the theoretical CDFs. The result of Donsker's Theorem (Donsker 1952) is that the convergence is inversely proportional to the square-root of the number of points forming the empirical distribution; i.e. the number of neurons N_E or N_I in this case. The upper panels in Fig. 4 display results with $N_E = N_I = 300$ and 2000, respectively.

The most pronounced impact of the different fluctuations in the empirical CDFs can be seen for small MFE magnitudes (small values of t), when comparing the I&F dynamics (red solid line) and the intersection of the SDE generated empirical CDFs (blue dashed line) in Fig. 4. These early exit times (the peaks close to $t = 0$ in Fig. 4) are governed by the fluctuations of the empirical CDFs, and thus we expect a discrepancy here in contrast to the later exit times (the peaks near to $t = 0.3$ in Fig. 4) which are governed by the mean of the process (i.e. the theoretical CDFs themselves). As we increase the number, k, of neurons initiating the MFE, the accuracy of the distribution created from the approximate empirical CDFs is improved since the boundary starts further away from the initial conditions, making early crossing less likely. In effect, we remove the part of the distribution that cannot be accurately resolved by the approximate empirical CDFs.

The other approximation we introduce is the analytical formula itself, approximating the first passage time distribution of the stochastic Brownian Bridge process to the moving boundary derived in Section 3.3. The distribution in Eq. (25), constructed from the two term approximation (32), which in turn is derived in a similar manner to that of Durbin (Durbin and Williams 1992), and thus we expect to have similar convergence. The error of this approximation can be seen in Fig. 4 by comparing the simulated SDE exit time distribution (blue dashed line) to the analytical formula (25) (green dashed line).

Finally, we investigate the validity of the analytical formula in approximating the true distribution of MFE magnitudes. For the parameters used in Figs. 4c and d, we compute the MFE magnitudes according to Eq. (35) in order to construct the MFE magnitude distributions. These distributions for both the number of excitatory and inhibitory neurons participating in the MFE agrees well with the corresponding

distributions obtained by resolving the original I&F dynamics (according to the method discussed in Ref. (Rangan and Young 2013a)) as shown in Fig. 5. As a result, the analytical formula (25) is a rather good approximation, capturing the bimodal nature of the MFE magnitude distributions.

5 Conclusions

Based on the cascade-induced synchrony in pulse-coupled I&F neuronal network models, we have explored how to obtain the distribution of the number of neurons firing together as part of a multiple firing event (MFE) from the voltage distributions of the excitatory and inhibitory populations. For population-based modeling (e.g., master equations or Fokker-Planck equations), this distribution provides a way to simulate dynamics in biologically relevant regimes which do not display homogeneous firing statistics. The method proposed in Ref. (Zhang et al. In preparation) involves stopping the evolution of the master equation, and then selecting the number of neurons to participate in an MFE. The analytical formula presented in this paper for the MFE magnitude distribution could be used in this step to improve computational efficiency.

The analytical formula for the MFE magnitude distribution accurately captures the bimodal nature of MFE sizes, revealing the strong competition between the excitatory and inhibitory neurons. Fluctuations in the distribution of neuronal voltages near threshold voltage can cause a very small sized MFE, or, if enough excitatory neurons fire initially, then a large sized MFE can ensue, involving a large fraction of both populations. It is these larger MFEs that characterize partial synchrony, and we are able to accurately capture these with the analytical formula. Further analysis of the analytical formula could provide more insight into the mechanism responsible for synchrony and provide a way to characterize partial synchrony as a function of coupling strengths as well as network size and voltage distributions.

The method we present in this paper is devised to capture the instantaneous MFEs produced by a current-based I&F model with infinitely-fast synaptic time-scales. These techniques can also be used to approximate the types of MFEs which manifest in spiking network models with nonzero synaptic rise and decay times. In this latter case the MFEs will not be instantaneous, but will still occur relatively quickly–typically lasting only 2–3 ms when the synaptic decay time-scales are 2–4 ms (see Ref. (Rangan and Young 2012) for some examples of these dynamic structures). How accurately these rapid transients will be captured by Eq. (32) depends on the ratio $r = \tau_E/\tau_I$ between the excitatory and inhibitory synaptic time-scales. When we derive Eq. (32) we assume that, while τ_E and τ_I both go to zero, $\tau_I < \tau_E$, thus giving the inhibitory synapses the potential to stifle excitation. When dealing with non-instantaneous synapses, if $r \sim 1$ we have a similar situation: the inhibitory firing events also have an opportunity to interfere with the excitatory cascade, and we expect Eq. (32) to be qualitatively accurate. However, when $r \ll 1$ we would expect Eq. (32) to underestimate the magnitude of the MFEs; synaptic excitation may transpire too quickly for inhibition to play a role, and the MFEs magnitude would be comparable to the all-excitatory case.

One of the limitations of our methodology is that we strongly rely on the assumption that our network is all-to-all coupled. Our approach does not directly generalize to more complicated network topologies; when the connectivity graph is nonuniform the simple picture painted in Fig. 2 breaks down.

Nevertheless, our work does illuminate how realistic synchronous burst sizes can be created by the competition between excitatory and inhibitory populations as opposed to complex network topology. We look forward to investigating how well this method describes other more realistic models and experimental data in future work.

Acknowledgments The authors would like to thank David Cai for useful discussions. J. Z. is partially supported by NSF grant DMS-1009575, K. N. is supported by the Courant Institute. D. Z. is supported by Shanghai Pujiang Program (Grant No. 10PJ1406300), NSFC (Grant No. 11101275 and No. 91230202), as well as New York University Abu Dhabi Research Grant G1301. A. R. is supported by NSF Grant DMS-0914827.

Appendixes

Appendix A: Firing events in I&F networks

In order to accurately simulate the dynamics of (1), we need to resolve the neurons' firing sequence correctly despite the fact that all neurons fire during the same instance of time in a single MFE. The algorithm used must produce an MFE magnitude consistent with the cascade condition (6) in Sec. 3.1. We present one such algorithm here in which the voltages of the remaining neurons are updated based on the neuron with the highest voltage first. We also emphasize that neurons having fired previously in an MFE do not receive input from neurons firing after it within the same MFE, because the neurons have a short refractory period, thus neurons can never fire more than once in an MFE.

To resolve the firing sequence of an MFE, we start from the sets $\{v_j\}_{j=1}^{N_E}$ and $\{w_j\}_{j=1}^{N_I}$ of the excitatory and

inhibitory neuronal voltages at the time one excitatory voltage is above threshold, indicating that this neuron is about to fire. Then, the following algorithm is used:

1. Find the k_E excitatory and k_I inhibitory voltages within the sets $\{v_j\}$ and $\{w_j\}$ that are above the threshold, V_T.
2. If both k_E and k_I are zero, stop; the MFE has ended. Otherwise, find the neuron with largest voltage, $V_{\max}$, out of the k_E excitatory and k_I inhibitory voltages above the threshold.
3. The neuron with voltage $V_{\max}$ fires; it is reset to V_R. If it is type E (I), it is removed from the list $\{v_j\}$ ($\{w_j\}$) and the remaining voltages of neurons that have not fired are updated by adding S^{EE} to (subtracting S^{EI} from) the voltages in $\{v_j\}$ and adding S^{IE} to (subtracting S^{II} from) the voltages in $\{w_j\}$.
4. If either set $\{v_j\}$ or $\{w_j\}$ is non-empty, return to Step 1. Otherwise, stop.

The MFE magnitudes for the excitatory and inhibitory populations are obtained by subtracting the number of neurons that did not fire in the MFE from the total numbers of neurons in the two populations,

$$m_E = N_E - \#\{v_j\} \quad \text{and} \quad m_I = N_I - \#\{w_j\}, \tag{36}$$

where # denotes the number of elements in the set. Note that the sets in Eq. (36) only include the voltages of non-firing neurons, as detailed in Step 3 of the algorithm.

Appendix B: Derivation of the geometric method

Starting from condition (6) in the main text, we describe here how to obtain a single condition, and therefore the MFE magnitude described by the single intersection point of $G(v)$ defined in Eq. (14) and the line $l(v)$ in Eq. (5). From the last points $v < V_T$ and $w < V_T$ where condition (6) is satisfied,

$$V_T - v = N_E S^{EE}(1 - F_E(v)) - N_I S^{EI}(1 - F_I(w)), \tag{37}$$
$$V_T - w = N_E S^{IE}(1 - F_E(v)) - N_I S^{II}(1 - F_I(w)), \tag{38}$$

we have

$$\frac{V_T - v}{N_E S^{EE}} = 1 - F_E(v) - \frac{N_I}{N_E}\frac{S^{EI}}{S^{EE}}(1 - F_I(w)), \tag{39}$$
$$\frac{V_T - w}{N_E S^{IE}} = 1 - F_E(v) - \frac{N_I S^{II}}{N_E S^{IE}}(1 - F_I(w)). \tag{40}$$

Subtracting Eq. (40) from Eq. (39) we have

$$\frac{V_T - v}{N_E S^{EE}} = \frac{V_T - w}{N_E S^{IE}} + \frac{N_I S^{II}}{N_E S^{IE}}(1 - F_I(w)) - \frac{N_I}{N_E}\frac{S^{EI}}{S^{EE}}(1 - F_I(w)),$$

which can be written as

$$v = V_T - (V_T - w)\frac{S^{EE}}{S^{IE}} - \delta N_I(1 - F_I(w)), \tag{41}$$

where $\delta = S^{II}S^{EE}/S^{IE} - S^{EI}$. The first two terms on the RHS suggest the transformation of the inhibitory voltages defined in Eq. (7) in the main text,

$$\hat{w} = V_T - (V_T - w)\frac{S^{EE}}{S^{IE}}. \tag{42}$$

This, together with the fact that one can show the empirical CDF

$$\begin{aligned} F_I(w) &= \int_{-\infty}^{w} \frac{1}{N_I}\sum_{j=1}^{N_I} \delta\left(\omega' - w_j\right) d\omega' \\ &= \int_{-\infty}^{\hat{w}} \frac{1}{N_I}\sum_{j=1}^{N_I} \delta\left(z - \hat{w}_j\right) dz \equiv \hat{F}_I(\hat{w}) \end{aligned} \tag{43}$$

allows Eq. (41) to be written as

$$v = \hat{w} - \delta N_I\left(1 - \hat{F}_I(\hat{w})\right). \tag{44}$$

Next, we must consider the two cases of $\delta > 0$ and $\delta < 0$ separately.

Case 1 If $\delta > 0$, we further transform $\hat{w}$ by

$$\bar{w} = \hat{w} - \delta N_I\left(1 - \hat{F}_I(\hat{w})\right), \tag{45}$$

appearing as Eq. (9) in the main text. Then, Eq. (44) is simply

$$v = \bar{w} \tag{46}$$

and we substitute this into Eq. (39), together with Eq. (43) to obtain

$$\frac{V_T - \bar{w}}{N_E S^{EE}} = 1 - F_E(\bar{w}) - \frac{N_I}{NE}\frac{S^{EI}}{S^{EE}}\left(1 - \hat{F}_I(\hat{w})\right). \tag{47}$$

What we want to do next is replace the function of $\hat{w}$ by a function of $\bar{w}$. Suppose we can invert the transformation $\bar{w} = \hat{w} - \delta N_I\left(1 - \hat{F}_I(\hat{w})\right)$ to obtain

$$\hat{w} = h(\bar{w}).$$

(Note that $h^{-1}(x) = x - \delta N_I(1 - \hat{F}_I(x))$, we have $\left[h^{-1}(x)\right]' = 1 + \hat{F}_I'(x) > 0$. Therefore, the transformation h is a monotonic increasing map and has only one root.) Then we have

$$\hat{F}_I(\hat{w}) = \int_{-\infty}^{\hat{w}} \frac{1}{N_I}\sum_{j=1}^{N_I} \delta\left(z - h(\bar{w}_j)\right) dz.$$

Changing the integration to the variable y defined by $y = h^{-1}(z)$, we have

$$\hat{F}_I(\hat{w}) = \int_{-\infty}^{\bar{w}} \frac{1}{N_I}\sum_{j=1}^{N_I} \delta\left(h(y) - h(\bar{w}_j)\right) h'(y) dy. \tag{48}$$

Taylor expanding $h(y)$ and only keeping the linear term, we have $h(y)-h(\bar{w}) = C_0(y-\bar{w})$ and $h'(y) = C_0$, resulting in

$$\hat{F}_I(\hat{w}) \approx \int_{-\infty}^{\bar{w}} \frac{1}{N_I}\sum_{j=1}^{N_I} \delta\left(C_0(y-\bar{w})\right) C_0 dy$$
$$= \frac{C_0}{|C_0|}\int_{-\infty}^{\bar{w}} \frac{1}{N_I}\sum_{j=1}^{N_I} \delta(y-\bar{w})dy \equiv \bar{F}_I(\bar{w}). \quad (49)$$

Substituting Eq. (49) into Eq. (47), we have

$$\frac{V_T-\bar{w}}{N_E S^{EE}} = 1 - F_E(\bar{w}) - \frac{N_I S^{EI}}{N_E S^{EE}}\left(1-\bar{F}_I(\bar{w})\right), \quad (50)$$

corresponding to Eq. (12) in the main text, where we defined $\bar{v} = v$ so that $\bar{F}_E(v) = F_E(v)$. Solving this for $\bar{w}$ is equivalent to finding the intersection point between the line $l(v) = 1 + \frac{1}{N_E S^{EE}}(v - V_T)$ and the function

$$G(v) = F_E(v) + \frac{N_I}{N_E}\frac{S^{EI}}{S^{EE}}\left(1-\bar{F}_I(v)\right) \text{ for } \delta \geq 0.$$

Case 2 If $\delta < 0$, then $\bar{w}$ defined in Eq. (45) may be larger than V_T, which we would like to avoid. Rather, we solve Eq. (44) for $\hat{w}$,

$$\hat{w} = v + \delta N_I\left(1-\hat{F}_I(\hat{w})\right) \quad (51)$$

and transform v to (Eq. (10) in the main text)

$$\bar{v} = v + \delta N_I\left(1-\hat{F}_I(\hat{w})\right) \quad (52)$$

so that Eq. (51) becomes

$$\bar{v} = \hat{w}. \quad (53)$$

Using Eq. (53) to rewrite Eq. (52) in terms of $\bar{v}$ and solving for v gives

$$v = \bar{v} - \delta N_I\left(1-\hat{F}_I(\bar{v})\right). \quad (54)$$

Using Eq. (54) and that $F_I(w) = \hat{F}_I(\hat{w})$, Eq. (40) becomes

$$\frac{V_T-\bar{v}}{N_E S^{EE}} = 1 - F_E(v) - \frac{N_I S^{II}}{N_E S^{IE}}\left(1-\hat{F}_I(\bar{v})\right), \quad (55)$$

corresponding to Eq. (12) in the main text, where we defined $\bar{w} = \hat{w}$, so that $\bar{F}_I(v) = \hat{F}_I(v)$.

Now, what we want to do is replace the function of v by a function of $\bar{v}$. If we denote Eq. (54) by

$$v = g(\bar{v}),$$

then change the integration variable in

$$F_E(v) = \int_{-\infty}^{v}\frac{1}{N_E}\sum_{j=1}^{N_E}\delta(z-v_j)dz$$

to y using $z = g(y)$ and $v_j = g(\bar{v}_j)$, we have that

$$F_E(v) = \int_{-\infty}^{\bar{v}}\frac{1}{N_E}\sum_{j=1}^{N_E}\delta\left(g(y)-g(\bar{v}_j)\right)g'(y)dy$$
$$\approx \int_{-\infty}^{\bar{v}}\frac{1}{N_E}\sum_{j=1}^{N_E}\delta\left(y-\bar{v}_j\right)dy \equiv \bar{F}_E(\bar{v})$$

following the same argument used to derive Eq. (49). Now, Eq. (55) becomes

$$\frac{V_T-\bar{v}}{N_E S^{EE}} = 1 - \bar{F}_E(\bar{v}) - \frac{N_I}{N_E}\frac{S^{II}}{S^{IE}}\left(1-\hat{F}_I(\bar{v})\right). \quad (56)$$

Solving this for $\bar{v}$ is equivalent to finding the intersection point between the line $l(v) = 1 + \frac{1}{N_E S^{EE}}(v - V_T)$ and the function

$$G(v) = \bar{F}_E(v) + \frac{N_I}{N_E}\frac{S^{II}}{S^{IE}}\left(1-\hat{F}_I(v)\right) \text{ for } \delta < 0.$$

Combining these two cases, we arrive at the MFE magnitude defined via the intersection of the function $G(v)$ defined in Eq. (14) in the main text, and the line $l(v)$ defined in Eq. (5) in the main text.

Appendix C: Analytical formula of first passage time

In this appendix, we explain how to reformulate the passage of a generic 2-dimensional anisotropic Brownian motion across a moving boundary to the viewpoint of one-dimensional Brownian motion as used in Durbin's papers (Durbin 1985; Durbin and Williams 1992).

We define $\mathbf{x} = (x, y)$ to be two-dimensional anisotropic brownian motion with linear drift, given by the solution to

$$dx = \alpha_x dt + \beta_x dW_t^X$$
$$dy = \alpha_y dt + \beta_y dW_t^Y$$

with initial starting point $\mathbf{x}(0) = \mathbf{0}$ for simplicity. If $\beta_x \neq \beta_y$, then we define the isotropic version of this process via $\mathbf{z} = (\hat{x}, \hat{y})$, with $\hat{x} = x/\beta_x$, $\hat{y} = y/\beta_y$, or $\mathbf{z} = \beta^{-1}\mathbf{x}$, with

$$\beta = \begin{bmatrix}\beta_x & 0\\ 0 & \beta_y\end{bmatrix}.$$

We will also define

$$\bar{\beta} = \begin{bmatrix}\beta_x & 0 & 0\\ 0 & \beta_y & 0\\ 0 & 0 & 1\end{bmatrix}.$$

We consider the first crossing density of $\mathbf{x}$ to a linear boundary $\mathcal{A}$ described by the normal constraint

$$\bar{\eta}\cdot(x, y, t) = k$$

where $\bar{\eta} = \left[\bar{\eta}_x, \bar{\eta}_y, \bar{\eta}_t\right]^\intercal$ is the unit normal to $\mathcal{A}$ in (x, y, t) space and k is the constant 'offset' of the linear plane (i.e., the distance between $\mathcal{A}$ and the origin $(0, 0, 0)$). We also

define $\eta_\perp = \left[\bar{\eta}_x, \bar{\eta}_y\right]^\mathsf{T}$ (not a unit vector) to be the projection of $\bar{\eta}$ onto the x, y plane. So we know the process $(x(t), y(t))$ crosses $\mathcal{A}$ when

$$\bar{\eta} \cdot (x(t), y(t), t) = k$$

or where

$$(\bar{\beta}\bar{\eta}) \cdot \left(\hat{x}, \hat{y}, t\right) = k$$

or when

$$\frac{\beta\eta_\perp}{|\beta\eta_\perp|} \cdot (\hat{x}, \hat{y}) = \frac{k - \bar{\eta}_t t}{|\beta\eta_\perp|}.$$

That is, $\mathbf{x}$ crosses $\mathcal{A}$ when $\mathbf{z}$ crosses $\bar{\beta}^{-1}\mathcal{A}$ (i.e., the boundary perpendicular to $\bar{\beta}\bar{\eta}$). Now $\mathbf{z}$ is isotropic brownian motion (plus a linear drift), so $\mathbf{z}$ can be described in terms of $z_\perp$ and $z_\parallel$, the directions parallel and perpendicular to $\eta_\perp$. Each of the processes $z_\perp$ and $z_\parallel$ are given by independent brownian motion (plus a linear drift). So the probability of $\mathbf{z}$ hitting the rescaled boundary $\bar{\beta}^{-1}\mathcal{A}$ at time t is just the probability of $z_\perp$ reaching the moving (scalar) boundary $\left[\bar{\beta}^{-1}\mathcal{A}\right]_\perp = (k - \bar{\eta}_t t) / |\beta\eta_\perp|$ at time t. That is to say

$$\begin{aligned} P(\mathbf{x} \text{ crosses } \mathcal{A} \text{ at time } t) &= P(\mathbf{z} \text{ crosses } \bar{\beta}^{-1}\mathcal{A} \text{ at time } t) \\ &= P\left(z_\perp \text{ crosses } \left[\bar{\beta}^{-1}\mathcal{A}\right]_\perp \right. \\ &\qquad \left. \text{at time } t\right). \end{aligned}$$

According to Durbin (1985), this probability is simply

$$\begin{aligned} &P\left(z_\perp \text{ crosses } \left[\bar{\beta}^{-1}\mathcal{A}\right]_\perp \text{ at time } t\right) \\ &= \left[\text{distance of } z_\perp \text{ to } \left[\bar{\beta}^{-1}\mathcal{A}\right]_\perp \text{ at time } 0\right] \frac{1}{t} \\ &\times \left[\text{density of } z_\perp \text{ on } \left[\bar{\beta}^{-1}\mathcal{A}\right]_\perp \text{ at time } t\right] \\ &= \frac{k}{|\beta\eta_\perp|}\frac{1}{t} \cdot \left[\text{density of } z_\perp \text{ on } \left[\bar{\beta}^{-1}\mathcal{A}\right]_\perp \text{ at time } t\right]. \end{aligned}$$

Now if $\mathbf{z}$ crosses at time t at a particular point $\bar{\beta}^{-1}a(t)$, then two things must happen. First, $z_\perp$ must equal $\left[\bar{\beta}^{-1}a(t)\right]_\perp$ which is also $(k - \bar{\eta}_t t) / |\beta\eta_\perp|$ at time t. Second, $z_\parallel$ must equal $\left[\bar{\beta}^{-1}a(t)\right]_\parallel$ at time t, where $\left[\bar{\beta}^{-1}a(t)\right]$ is the component of $a(t)$ perpendicular to $\eta_\perp$. Thus, the probability that the process $\mathbf{z}$ crosses at time t at a particular point $\bar{\beta}^{-1}a(t)$ on $\bar{\beta}^{-1}\mathcal{A}$ is given by

$$\begin{aligned} &P(t, \mathbf{z} \text{ crosses at } \bar{\beta}^{-1}a(t)) \\ &= P\left(z_\perp \text{ crosses } \left[\bar{\beta}^{-1}\mathcal{A}\right]_\perp \text{ at time } t\right) \\ &\times P\left(z_\parallel \text{ is equal to } [\bar{\beta}^{-1}a(t)]_\parallel \text{ at time } t\right). \end{aligned}$$

Now, as we discussed above,

$$\begin{aligned} &P\left(z_\perp \text{ crosses } [\bar{\beta}^{-1}\mathcal{A}]_\perp \text{ at time } t\right) \\ &= \frac{k}{|\beta\eta_\perp|}\frac{1}{t} \cdot \left[\text{density of } z_\perp \text{ on } [\bar{\beta}^{-1}a(t)]_\perp \text{ at time } t\right]. \end{aligned}$$

For the second term, we have

$$\begin{aligned} &P\left(z_\parallel \text{ is equal to } \left[\bar{\beta}^{-1}a(t)\right]_\parallel \text{ at time } t\right) \\ &= \left[\text{density of } z_\parallel \text{ on } [\bar{\beta}^{-1}a(t)]_\parallel \text{ at time } t\right], \end{aligned}$$

and together, since $z_\perp$ and $z_\parallel$ are independent,

$$\begin{aligned} &P(t, \mathbf{z} \text{ crosses at } \bar{\beta}^{-1}a(t)) \\ &= \frac{k}{|\beta\eta_\perp|}\frac{1}{t} \cdot \left[\text{density of } \mathbf{z} \text{ on } \left[\bar{\beta}^{-1}a(t)\right] \text{ at time } t\right]. \end{aligned}$$

As we discussed above, if $\mathbf{z}$ crosses at time t at a point $\bar{\beta}^{-1}a(t)$, then $\mathbf{x}$ crosses at time t at $a(t)$. However, the density $p\left(t, \mathbf{z} \text{ crosses at } \bar{\beta}^{-1}a(t)\right)$ is not equivalent to the density $p(t, \mathbf{x} \text{ crosses at } a(t))$. Rather, we have

$$\begin{aligned} &P\left(t, \mathbf{z} \text{ crosses the line-segment } \right. \\ &\qquad \left. \left[\bar{\beta}^{-1}a(t), \bar{\beta}^{-1}(a(t) + \delta \cdot \bar{\eta}_\parallel)\right]\right) \\ &= P\left(t, \mathbf{x} \text{ crosses the line-segment } \left[a(t), a(t) + \delta \cdot \bar{\eta}_\parallel\right]\right), \end{aligned}$$

where $\bar{\eta}_\parallel = \left[-\bar{\eta}_y, \bar{\eta}_x, 0\right]^\mathsf{T}$, and $\eta_\parallel = \left[-\bar{\eta}_y, \bar{\eta}_x\right]^\mathsf{T}$ (not a unit vector) lies along $\mathcal{A}$ and lies in the x-y plane, and is perpendicular to $\eta_\perp$. Comparing the lengths of these line segments, we see that length $\left|\bar{\beta}^{-1}a(t), \bar{\beta}^{-1}(a(t) + \delta \cdot \bar{\eta}_\parallel)\right| = \delta \cdot \left|\beta^{-1}\eta_\parallel\right|$ and length $\left|a(t), a(t) + \delta \cdot \bar{\eta}_\parallel\right| = \delta \cdot \left|\eta_\parallel\right|$. Using this relationship we can conclude the density

$$\begin{aligned} &p\left(t, \mathbf{z} \text{ crosses at } \bar{\beta}^{-1}a(t)\right) \frac{\left|\beta^{-1}\eta_\parallel\right|}{\left|\eta_\parallel\right|} \\ &= p(t, \mathbf{x} \text{ crosses at } a(t)). \end{aligned}$$

This in turn implies that the probability that the process $\mathbf{x}$ crosses $\mathcal{A}$ at time t at a particular point $a(t)$ on $\mathcal{A}$ is given by the density

$$\begin{aligned} p(t, \mathbf{x} \text{ crosses at } \mathbf{a}) &= \frac{\left|\beta^{-1}\eta_\parallel\right|}{\left|\eta_\parallel\right|}\frac{k}{|\beta\eta_\perp|}\frac{1}{t} \\ &\times \left[\text{density of } \mathbf{z} \text{ on } [\bar{\beta}^{-1}a(t)] \text{ at time } t\right]. \end{aligned}$$

Finally, since

$$\begin{aligned} &\left[\text{density of } \mathbf{z} \text{ on } \left[\bar{\beta}^{-1}a(t)\right] \text{ at time } t\right] |\beta|^{-1} \\ &\qquad = \left[\text{density of } \mathbf{x} \text{ on } a(t) \text{ at time } t\right], \end{aligned}$$

where $|\beta|$ is the determinant of β. The density

$$\begin{aligned} p(t, \mathbf{x} \text{ crosses at } \mathbf{a}) &= \frac{\left|\beta^{-1}\eta_\parallel\right|}{\left|\eta_\parallel\right|}\frac{k}{|\beta\eta_\perp|}\frac{1}{t} \\ &\times |\beta| \left[\text{density of } \mathbf{x} \text{ on } a(t) \text{ at time } t\right]. \end{aligned}$$

Using the language described in Section 3.3, the above can be written as

$$p(t,\mathbf{a}|0,\mathbf{x}(0)) = \frac{1}{t-0}\left(\widehat{\mathcal{A}}_{a(t)}|_0 - \mathbf{x}(0)\right)\cdot\eta_\perp \times \frac{\left|\beta^{-1}\eta_\parallel\right|}{|\beta\cdot\eta_\perp|}\frac{|\beta|}{|\eta_\perp|\left|\eta_\parallel\right|} f(t,\mathbf{a}|0,\mathbf{x}(0)),$$

leading to

$$p(t,\mathbf{a}) = \lim_{s\to t^-}\frac{f(t,\mathbf{a})}{t-s}\int_{\partial\Omega(s)}\left(\widehat{\mathcal{A}}_{a(t)}|_s - \mathbf{x}\right)\cdot n_\perp \times \frac{\left|\beta^{-1}n_\parallel\right|}{|\beta n_\perp|}\frac{|\beta|}{|n_\perp|\left|n_\parallel\right|} g(s,\mathbf{x}|t,\mathbf{a})\,d\mathbf{x}, \tag{57}$$

where $f(t,\mathbf{a}|0,\mathbf{x}(0))$ is a (unconditioned) density for the process $\mathbf{x}$ at t, $\mathbf{a}$, see details in Appendix B.

We can now fill in the geometry for the specific problem at hand. The points (x, y) on the surface $\mathcal{A}$ at time t was given in Eq. (23) and comes from the constraint of $\bar{G}(t) = \bar{I}(t)$. The vector

$$\eta = \left[-\gamma, \alpha, \alpha\bar{p}_I(t) - \gamma\bar{p}_E(t) + \frac{1}{N_E S^{EE}}\right]$$

is normal to the surface in 3D space at the point (x, y, t). The 2-component normal to $\mathcal{A}$, restricted to the x-y plane, is

$$n_\perp = \frac{1}{|\eta|}\eta_\perp = \frac{1}{|\eta|}[-\gamma,\alpha],$$

and the 2-component vector perpendicular to $n_\perp$ is

$$n_\parallel = \frac{1}{|\eta|}\eta_\parallel = \frac{1}{|\eta|}[\alpha,\gamma]$$

where $|\eta|$ is the length of the vector η. One can also think of $\mathcal{A}$ as a line parallel to $-\gamma x + \alpha y$ in the x-y plane, with a time dependent offset of $k/N_E + \gamma\bar{f}_E(t) - \alpha\bar{f}_I(t) - \frac{1}{N_E S^{EE}}t$. So, around any point $(\mathbf{a}(t), t) = \left(a_x, a_y, t\right)$ on $\mathcal{A}$, the point

$$\widehat{\mathcal{A}}_{a(t)}|_s = \mathbf{a} - \mathbf{u}\,\nu_n(t)(t-s)$$

is on the linearized boundary tangent to $\mathcal{A}$ at the point $\mathbf{a}(t)$. The factor

$$\nu_n(t) = \sqrt{\gamma^2+\alpha^2}\left(\alpha\bar{\rho}_I(t) - \gamma\bar{\rho}_E(t) + \frac{1}{N_E S^{EE}}\right)^{-1} \tag{58}$$

can be thought of as the speed at which the boundary propagates in the normal direction, as s (and hence $t-s$) changes and the unit vector in the x-y plane $\mathbf{u} = \frac{[-\gamma,\alpha]}{\sqrt{\gamma^2+\alpha^2}}$ is perpendicular to $\widehat{\mathcal{A}}$ and therefore parallel to $n_\perp$. Therefore,

$$\frac{\widehat{\mathcal{A}}_{a(t)}|_s - \mathbf{a}}{t-s} = -\mathbf{u}\,\nu_n(t).$$

We now change variables to the $n_\perp$ and $n_\parallel$ directions by first changing to variables in which the stochastic processes $(\phi_E(t), \phi_I(t))$ obeys isotropic Brownian motion in 2D. This is done with the matrix

$$\beta = \begin{pmatrix}\sqrt{\frac{\bar{p}_E(t)}{N_E}} & 0\\ 0 & \sqrt{\frac{\bar{p}_I(t)}{N_I}}\end{pmatrix}$$

and requires the change of variables term given by

$$n_\perp\frac{\left|\beta^{-1}n_\parallel\right|}{|\beta n_\perp|}\frac{|\beta|}{|n_\perp|\left|n_\parallel\right|} = \mathbf{u}\sqrt{1+1/\nu_n^2} = \mathbf{u}\,\zeta,$$

where $\zeta = \sqrt{1+1/\nu_n^2}$.

Using the definition $l(s,\mathbf{x}|t,\mathbf{a}) = \left(\widehat{\mathcal{A}}_{a(t)}|_s - \mathbf{x}\right)\cdot\mathbf{u}\,\zeta$, we can calculate the density of crossing at time t and position $\mathbf{a}$ on $\mathcal{A}$ via

$$\begin{aligned} &p(t,\mathbf{a})\\ &= \lim_{s\to t^-}\frac{f(t,\mathbf{a})}{t-s}\mathbb{E}(l(s,\mathbf{x}|t,\mathbf{a})|\text{ first crossing at } t,\mathbf{a})\\ &= \lim_{s\to t^-}\frac{f(t,\mathbf{a})}{t-s}\mathbb{E}(l(s,\mathbf{x}|t,\mathbf{a})|\text{ some crossing at } t,\mathbf{a})\\ &- \lim_{s\to t^-}\frac{f(t,\mathbf{a})}{t-s}\mathbb{E}(l(s,\mathbf{x}|t,\mathbf{a})|\text{ crossing at } t,\mathbf{a}\\ &\qquad\text{and a first crossing at } (r,\mathbf{b}) \text{ where } r<t). \end{aligned} \tag{59}$$

In the above expression the term $f(t,\mathbf{a})$ refers to the unconditioned density of the process (ϕ_E,ϕ_I,t) at time t and position $\mathbf{a}$ (presumed to lie on $\mathcal{A}$). The first term in the sum is straightforward, the second term is a little trickier. Note that the conditional first passage density at time r to point $\mathbf{b}$ given that the process also crosses the point $\mathbf{a}$ at time t can be written as $q(r,\mathbf{b})f(r,\mathbf{b}|t,\mathbf{a}) = q(r,\mathbf{b})f(r,\mathbf{b},t,\mathbf{a})/f(t,\mathbf{a})$, where $q(r,\mathbf{b})$ is defined via $p(r,\mathbf{b}) = q(r,\mathbf{b})f(r,\mathbf{b})$. Following Durbin's method, we achieve the analytical formula (32) by taking the first two terms of Eq. (59) in the main text.

Appendix D: Probability density of stochastic process

In this appendix, we derive the distributions $f(t,\mathbf{a})$ in Eq. (33) and $f(r,\mathbf{b}|t,\mathbf{a})$ in Eq. (34) in the main text. Recall that $\bar{f}_E(t)$ and $\bar{f}_I(t)$ are the smooth CDFs for the transformed voltage variables, defined in Eq. (18). These define the stochastic processes $\phi_E(t)$ and $\phi_I(t)$ in Eq. (20).

The distribution $f(t,\mathbf{a})$ refers to the probability of observing the unconstrained process (ϕ_E,ϕ_I) at $\mathbf{a}(t)$ at time t. In other words, $f(t,\mathbf{a})$ is the probability that

$$\phi(t) = \begin{bmatrix}\phi_E(t)\\ \phi_I(t)\end{bmatrix} = \mathbf{a}(t) = \begin{bmatrix}a_E(t)\\ a_I(t)\end{bmatrix}$$

at time t, without assuming anything about how ϕ crosses $\mathcal{A}$. This probability is given by:

$$f(t,\mathbf{a}) = P(\phi_E(t) = a_E(t))\,P(\phi_I(t) = a_I(t)),$$

where each component of ϕ evolves independently. Now of course the probability that $\phi_Q(t) = a_Q(t)$ at the time t is the same as the probability that $\bar{\phi}_Q(\tau) = a_Q(t)$ at time $\tau = f_Q(t)$. This in turn is the same as $\sqrt{N_Q}$ times the probability $P\left(B_\tau = \sqrt{N_Q}a_Q\right)$, the probability that a standard brownian bridge (connecting $(0,0)$ to $(1,0)$) reaches the value $\sqrt{N_Q}a_Q(t)$ at time $\tau = f_Q(t)$. According to Durbin and Williams (1992), this probability is given by

$$P\left(B_\tau = \sqrt{N_Q}a_Q\right) = \frac{1}{\sqrt{2\pi\,\tau\,(1-\tau)}}\exp\left(-\frac{1}{2}\frac{N_Q {a_Q}^2}{\tau\,(1-\tau)}\right)$$

therefore $f(t, \mathbf{a})$ is precisely Eq. (33) in the main text.

In a similar vein the distribution $f(r, \mathbf{b}|t, \mathbf{a})$ is the conditional distribution of the process ϕ at $r, \mathbf{b}$, given that the point $t, \mathbf{a}$ is reached. Using logic similar to the above, this is given by

$$\begin{aligned}
&f(r, \mathbf{b}|t, \mathbf{a}) = P\left(\phi_E(r) = b_E(r) \mid \phi_E(t) = a_E(t)\right)\\
&\times P\left(\phi_I(r) = b_I(r) \mid \phi_I(t) = a_I(t)\right)\\
&= P\left(\bar{\phi}_E(\bar{f}_E(r)) = b_E(r) \mid \bar{\phi}_E(\bar{f}_E(t)) = a_E(t)\right)\\
&\times P\left(\bar{\phi}_I(\bar{f}_I(r)) = b_I(r) \mid \bar{\phi}_I(\bar{f}_I(t)) = a_I(t)\right)\\
&= \sqrt{N_E}P\left(B_{f_E(r)} = \sqrt{N_E}b_E \mid B_{f_E(t)} = \sqrt{N_E}a_E\right)\\
&\times\sqrt{N_I}P\left(B_{f_I(r)} = \sqrt{N_I}b_I \mid B_{f_I(t)} = \sqrt{N_I}a_I\right).
\end{aligned}$$

Note that B_τ conditioned to hit $\sqrt{N_Q}a_Q$ at time $f_Q(t)$ is just a brownian bridge connecting $(0,0)$ to $(f_Q(t), \sqrt{N_Q}a_Q)$. One can think of this new brownian bridge as a rescaled version of a standard brownian bridge:

$$\begin{aligned}
&P(B_r = x \mid B_t = a \mid B_1 = 0) = P(B_r = x \mid B_t = a)\\
&= P\left(B_r - a\frac{r}{t} = x - a\frac{r}{t} \mid B_t - a\frac{t}{t} = 0\right)\\
&= P\left(B_{r/t} = x - a\frac{r}{t} \mid B_1 = 0\right)\\
&= \frac{1}{\sqrt{2\pi\frac{r}{t}\left(1-\frac{r}{t}\right)}}\exp\left(-\frac{1}{2}\frac{\left[x - a\frac{r}{t}\right]^2}{\frac{r}{t}\left(1-\frac{r}{t}\right)}\right).
\end{aligned}$$

Then

$$\begin{aligned}
&P\left(B_{f_Q(r)} = \sqrt{N_Q}b_Q \mid B_{f_Q(t)} = \sqrt{N_Q}a_Q\right)\\
&= \frac{f_Q(t)}{\sqrt{2\pi f_Q(r)\left(f_Q(t) - f_Q(r)\right)}}\\
&\exp\left(-\frac{1}{2}\frac{N_Q\left[b_Q f_Q(t) - a_Q f_Q(r)\right]^2}{f_Q(r)(f_Q(t) - f_Q(r))}\right)
\end{aligned}$$

and formula (34) for $f(r, \mathbf{b}|t, \mathbf{a})$ in the main text follows. In the computation of MFE magnitude, we must simply account for not selecting the k neurons that initiate the MFE, so we replace N_E by $N_E - k$.

References

Amari, S. (1974). A method of statistical neurodynamics. *Kybernetik*, *14*, 201–215.

Amit, D., & Brunel, N. (1997). Model of global spontaneous activity and local structured activity during delay periods in the cerebral cortex. *Cerebral Cortex*, *7*, 237–252.

Anderson, J., Carandini, M., Ferster, D. (2000). Orientation tuning of input conductance, excitation, and inhibition in cat primary visual cortex. *Journal of Neurophysiology*, *84*, 909–926.

Battaglia, D., & Hansel, D. (2011). Synchronous chaos and broad band gamma rhythm in a minimal multi-layer model of primary visual cortex. *PLoS Computational Biology*, *7*(10), e1002176.

Benayoun, M., Cowan, J.V., Drongelen, W., Wallace, E. (2010). Avalanches in a stochastic model of spiking neurons. *PLoS Computational Biology*, *6*(7), e1002176.

Brette, R., Rudolph, M., Carnevale, T., Hines, M., Beeman, J., Bower, J., Diesmann, M., Morrison, A., Goodman, P., Harris JR., F., et al. (2007). Simulation of networks of spiking neurons: a review of tools and strategies. *Journal of Computational Neuroscience*, *23*(3), 349–398.

Brunel, N. (2000). Dynamics of sparsely connected networks of excitatory and inhibitory spiking neurons. *Journal of Computational Neuroscience*, *8*, 183–208.

Brunel, N., & Hakim, V. (1999). Fast global oscillations in networks of integrate-and-fire neurons with low firing rates. *Neural Computation*, *11*, 1621–1671.

Bruzsaki, G., & Draguhn, A. (2004). Neuronal oscillations in cortical networks. *Science*, *304*, 1926–1929.

Cai, D., Tao, L., Shelley, M., McLaughlin, D. (2004). An effective kinetic representation of fluctuation-driven neuronal networks with application to simple and complex cells in visual cortex. *Proceedings of the National Academy of Science*, *101*(20), 7757–7762.

Cai, D., Rangan, A., McLaughlin, D. (2005). Architectural and synaptic mechanisms underlying coherent spontaneous activity in V1. *Proceedings of the National Academy of Science*, *102*(16), 5868–5873.

Cai, D., Tao, L., Rangan, A. (2006). Kinetic theory for neuronal network dynamics. *Communications Mathematical Sciences*, *4*, 97–127.

Cardanobile, S., & Rotter, S. (2010). Multiplicatively interacting point processes and applications to neural modeling. *Journal of Computational Neuroscience*, *28*, 267–284.

Churchland, M.M., et al., et al. (2010). Stimulus onset quenches neural variability: a widespread cortical phenomenon. *Nature Neuroscience*, *13*(3), 369–378.

DeVille, R., & Peskin, C. (2008). Synchrony and asynchrony in a fully stochastic neural network. *Bulletin of Mathematical Biology*, *70*(6), 1608–33.

DeWeese, M., & Zador, A. (2006). Non-gaussian membrane potential dynamics imply sparse, synchronous activity in auditory cortex. *Journal of Neuroscience*, *26*(47), 12,206–12,218.

Donsker, M. (1952). Justification and extension of Doobs heuristic approach to the Kolmogorov-Smirnov theorems. *Annals of Mathematical Statistics*, *23*(2), 277–281.

Durbin, J. (1985). The first passage density of a continuous Gaussian process to a general boundary. *Journal of Applied Probability*, *22*, 99–122.

Durbin, J., & Williams, D. (1992). The first passage density of the brownian process to a curved boundary. *Journal of Applied Probability*, *29*, 291–304.

Eggert, J., & Hemmen, J. (2001). Modeling neuronal assemblies: theory and implementation. *Neural Computation*, *13*, 1923–1974.

Fusi, S., & Mattia, M. (1999). Collective behavior of networks with linear integrate and fire neurons. *Neural Computation*, *11*, 633–652.

Gerstner, W. (1995). Time structure of the activity in neural network models. *Physical Review E*, *51*, 738–758.

Gerstner, W. (2000). Population dynamics of spiking neurons: fast transients, asynchronous states and locking. *Neural Computation*, *12*, 43–89.

Hansel, D., & Sompolinsky, H. (1996). Chaos and synchrony in a model of a hypercolumn in visual cortex. *Journal of Computational Neuroscience*, *3*, 7–34.

Knight, B. (1972). Dynamics of encoding in a population of neurons. *Journal of General Physiology*, *59*, 734–766.

Kriener, B., Tetzlaff, T., Aertsen, A., Diesmann, M., Rotter, S. (2008). Correlations and population dynamics in cortical networks. *Neural Computation*, *20*, 2185–2226.

Krukowski, A., & Miller, K. (2000). Thalamocortical NMDA conductances and intracortical inhibition can explain cortical temporal tuning. *Nature Neuroscience*, *4*, 424–430.

Lampl, I., Reichova, I., Ferster, D. (1999). Synchronous membrane potential fluctuations in neurons of the cat visual cortex. *Neuron*, *22*, 361–374.

Lei, H., Riffell, J., Gage, S., Hildebrand, J. (2009). Contrast enhancement of stimulus intermittency in a primary olfactory network and its behavioral significance. *Journal of Biology*, *8*, 21.

Mazzoni, A., Broccard, F., Garcia-Perez, E., Bonifazi, P., Ruaro, M., Torre, V. (2007). On the dynamics of the spontaneous activity in neuronal networks. *PLoS One*, *2*(5), e439.

Murthy, A., & Humphrey, A. (1999). Inhibitory contributions to spatiotemporal receptive-field structure and direction selectivity in simple cells of cat area 17. *Journal of Neurophysiology*, *81*, 1212–1224.

Newhall, K., Kovačič, G., Kramer, P., Cai, D. (2010). Cascade-induced synchrony in stochastically driven neuronal networks. *Physical Review E*, *82*, 041903.

Nykamp, D., & Tranchina, D. (2000). A population density approach that facilitates large scale modeling of neural networks: analysis and application to orientation tuning. *Journal of Computational Neuroscience*, *8*, 19–50.

Omurtage, A., Knight, B., Sirovich, L. (2000). On the simulation of a large population of neurons. *Journal of Computational Neuroscience*, *8*, 51–63.

Petermann, T., Thiagarajan, T., Lebedev, M., Nicolelis, M., Chailvo, D., Plenz, D. (2009). Spontaneous cortical activity in awake monkeys composed of neuronal avalanches. *Proceedings of the National Academy of Science*, *106*, 15,921–15,926.

Rangan, A., & Cai, D. (2007). Fast numerical methods for simulating large-scale integrate-and-fire neuronal networks. *Journal of Computational Neuroscience*, *22*(1), 81–100.

Rangan, A., & Young, L. (2012). A network model of V1 with collaborative activity. PNAS Submitted.

Rangan, A., & Young, L. (2013a). Dynamics of spiking neurons: between homogeneity and synchrony. *Journal of Computational Neuroscience*, *34*(3), 433–460. doi:10.1007/s10827-012-0429-1.

Rangan, A., & Young, L. (2013b). Emergent dynamics in a model of visual cortex. *Journal of Computational Neuroscience*. doi:10.1007/s10827-013-0445-9.

Renart, A., Brunel, N., Wang, X. (2004). Mean field theory of irregularly spiking neuronal populations and working memory in recurrent cortical networks. *Computational Neuroscience: A comprehensive approach*.

Riffell, J., Lei, H., Hildebrand, J. (2009a). Neural correlates of behavior in the moth Manduca sexta in response to complex odors. *Proceedings of the National Academy of Science*, *106*, 19,219–19,226.

Riffell, J., Lei, H., Christensen, T., Hildebrand, J. (2009b). Characterization and coding of behaviorally significant odor mixtures. *Current Biology*, *19*, 335–340.

Samonds, J., Zhou, Z., Bernard, M., Bonds, A. (2005). Synchronous activity in cat visual cortex encodes collinear and cocircular contours. *Journal of Neurophysiology*, *95*, 2602–2616.

Sillito, A. (1975). The contribution of inhibitory mechanisms to the receptive field properties of neurons in the striate cortex of the cat. *Journal of Physiology*, *250*, 305–329.

Singer, W. (1999). Neuronal synchrony: a versatile code for the definition of relations? *Neuron*, *24*, 49–65.

Sompolinsky, H., & Shapley, R. (1997). New perspectives on the mechanisms for orientation selectivity. *Current Opinion in Neurobiology*, *7*, 514–522.

Sun, Y., Zhou, D., Rangan, A., Cai, D. (2010). Pseudo-Lyapunov exponents and predictability of Hodgkin-Huxley neuronal network dynamics. *Journal of Computational Neuroscience*, *28*, 247–266.

Treves, A. (1993). Mean-field analysis of neuronal spike dynamics. *Network*, *4*, 259–284.

Wilson, H., & Cowan, D. (1972). Excitatory and inhibitory interactions in localized populations of model neurons. *Biophysical Journal*, *12*, 1–24.

Wilson, H., & Cowan, D. (1973). A Mathematical theory of the functional dynamics of cortical and thalamic nervous tissue. *Kybernetik*, *13*, 55–80.

Worgotter, F., & Koch, C. (1991). A detailed model of the primary visual pathway in the cat comparison of afferent excitatory and intracortical inhibitory connection schemes for orientation selectivity. *Journal of Neuroscience*, *11*, 1959–1979.

Yu, Y., & Ferster, D. (2010). Membrane potential synchrony in primary visual cortex during sensory stimulation. *Neuron*, *68*, 1187–1201.

Yu, S., Yang, H., Nakahara, H., Santos, G., Nikolic, D., Plenz, D. (2011). Higher-order interactions characterized in cortical activity. *Journal of Neuroscience*, *31*, 17,514–17,526.

Zhang, J., Rangan, A., Cai, D., et al. (In preparation). A coarse-grained framework for spiking neuronal networks: between homogeneity and synchrony.

Zhou, D., Sun, Y., Rangan, A., Cai, D. (2008). Network induced chaos in integrate-and-fire neuronal ensembles. *Physical Review E*, *80*(3), 031918.